SAND2005-6077

Electrodeposition of Nickel from Low Temperature Sulfamate Electrolytes

Part I: Electrochemistry and Film Stress

Part II: Properties and Structure of Electrodeposits

S. H. Goods, J. J. Kelly**, A. A. Talin, J. R. Michael*, R. Watson, J. Hachman

Physical and Engineering Science Center and

*Materials and Process Sciences Center

To be published in:

The *Journal of Electrochemical Society*

**Current Address: IBM/T.J. Watson Research Center
Yorktown Heights, NY 10598

Electrodeposition of Nickel From Low Temperature Sulfamate Electrolytes Part I: Electrochemistry and Film Stress

J. J. Kelly**, S. H. Goods, A. A. Talin, , J. Hachman

Sandia National Laboratories
*Livermore, CA 94551

**IBM/T.J. Watson Research Center
Yorktown Heights, NY 10598

Abstract

The film stress of Ni films deposited at near-ambient temperatures from sulfamate electrolytes was studied. The particulate filtering of the electrolyte, a routine industrial practice, becomes an important deposition parameter at lower bath temperatures. At 28 °C, elevated tensile film stress develops at low current densities (<10 mA/cm^2) if the electrolyte is filtered. Filtering at higher current densities has a negligible effect on film stress. A similar though less pronounced trend is observed at 32 °C. Sulfate-based Ni plating baths display similar film stress sensitivity to filtering, suggesting that this is a general effect for Ni electrodeposition. It is shown that filtering does not significantly change the current efficiency or the pH near the surface during deposition. The observed changes in film stress are thus attributed not to adsorbed hydrogen but instead to the effects of filtering on the formation and concentration of polyborate species due to the decreased solubility of boric acid at near-ambient temperatures.

Introduction

The electrodeposition of nickel from sulfamate electrolytes is an industrially important process.[1] The sulfamate chemistry is often preferred due to low deposited film stress (even without S-bearing organic additives),[2-4] the low sulfur content of the deposited metal,[5] and the generally good mechanical properties of the Ni.[6-9] Additionally, the high current efficiency of the bath typically allows for high deposition rates (>100 mA/cm^2), permitting the rapid deposition of thick, low-stress films. These electrolytes have been effectively employed for years in the bulk electroforming of structural components, wear resistant coatings, and stamping/embossing tools.[1-8]

More recently, the sulfamate bath has become a popular choice for the through-mask electrodeposition of microsystem components using LIGA* or LIGA-like processes.[9] Since many such-fabricated microcomponents perform mechanical functions, the microstructure and mechanical properties of the microfabricated Ni structures are of interest, as well as the deposition conditions that may affect them. While the process-structure-property relationships are generally known for Ni sulfamate baths under typical operating conditions,[10-11] the successful integration of the electrodeposition step with other steps in the LIGA process (or other microfabrication processes involving plating through a lithographic mask) may necessitate deposition conditions that differ from standard plating practice.

First, low bath temperatures may be preferred to minimize the thermal expansion of the resist material (typically polymethylmethacralate or PMMA) used in the LIGA process. Since the lateral part dimensions are defined by the PMMA resist, any dimensional errors in the resist (due to PMMA thermal expansion in the plating bath, or swelling from water uptake) is replicated by the electroformed part. Low electrolyte temperatures thus improve the dimensional fidelity of the final LIGA parts. Additionally, low current densities are generally employed for high aspect ratio features in thick molds to avoid transport limitations. However, experimental studies with sulfamate electrolytes under these conditions are few in number.[12] In this first part, we study the film stress of sulfamate-deposited Ni at low current densities and low bath temperatures, as well as the current efficiencies and pH values near the deposition surface. In a second part, the effects of these conditions on the film microstructure and mechanical properties will be presented.

* German acronym for lithography, electroplating, and molding

Experimental

The composition of the electrolyte was fixed at 1.35 M $Ni(SO_3NH_2)_2$ (hereafter referred to as Ni-sulfamate), 30 g/L boric acid, and 0.2 g/L sodium dodecyl sulfate (SDS, a wetting agent that reduces pitting and otherwise has no effect on the Ni)[13] unless as noted. Ni-sulfamate solution was obtained as a 3.12 M aqueous solution from Atotech (Electropure 24, Germany). All other chemicals were from Fisher and were of ACS reagent grade. Manufacturers generally recommend increasing boric acid concentration from 30 g/L to 45 g/L as the bath temperature is raised from 32 to 50 °C, (no boric acid concentration recommendation is made for lower temperatures). In the present study, a bath temperature of 28 °C was typically employed, although other temperatures were investigated as indicated. This temperature was chosen to minimize thermal expansion and loss of dimensional fidelity in the thick PMMA photoresist used to defined the throughmold structures in the LIGA process.[14] It should be noted that this temperature is somewhat lower than the minimum of 32 °C recommended by most Ni-sulfamate manufacturers. The implications of this choice will be discussed later. A pH of 3.5 ± 0.1 was used for all experiments; the typically recommended range is from 3.5 to 4.5. Additions of sulfamic acid were made to decrease pH as necessary.

S-depolarized Ni S-Rounds (Inco, Canada) contained in a Ti basket served as the anode. For unfiltered solutions, a 1 L glass beaker was used as the reaction cell, while for filtered solutions a liquid chromatography glass jar (Fisher) with a volume of 4 L was employed; the higher volume was necessary to accommodate the filtering pump described below. It was verified that the different cell volumes had no impact on the experimental results.

Stock sulfamate electrolytes were purified by passage through activated carbon using an in-tank filtering pump and activated C cartridge (Floking, FL) for various periods of time as indicated. The volume of the stock solution was 7 L. This volume was convenient for the C treatment and also ensured that all of the solution would be used within a few weeks of the purification. The purification occurred at the as-received pH of about 4.5. It will be shown that this initial carbon treatment is important to ensure reproducible stress results. The maximum flow rate of the in-tank pump was about 10 L/min, but the use of a particle filter reduced this somewhat. Wound, 5 μm polypropylene fiber filters were used (Floking).

Film stress was measured using a bent strip method described elsewhere.[15] The deposition time for each current density investigated was varied to keep the total charge constant, resulting in a nominal film thickness of 1 μm for each measurement. This allowed for the comparison of stress results for different current densities. A constant current source accurate to 0.1 mA was used to deposit the Ni films for stress measurements. Polarization curves were obtained using a Pine rotator and Pt disk electrode (New Jersey) with an Autolab PGSTAT 12 potentiostat (Holland).

The pH near the cathode surface was investigated using a Au mesh working electrode (Internet, Inc., Minneapolis, MN) and flat-bottomed pH electrode (Omega); this technique has been discussed in some detail in the literature.[16-18] During the measurement, the bulk solution was quiescent; in between measurements, the solution was well-mixed by a stir bar. Although no stirring was used during the measurement, it was verified that bulk stirring had no effect on the pH signal. Reported pH values correspond to the average value in a stable plateau that the pH reached after approximately one minute. The mesh size was 500, corresponding to a Au wire diameter of about 17 μm spaced about 33 μm apart. The validity of this approach in capturing conditions at the cathode surface has been discussed previously[16-18] and we believe it is a useful technique for the present study.

Results and Discussion

Carbon Treatment

Figures 1a and b show the effect of C treatment on the deposited film stress as a function of current density (Figure 1a) for unfiltered 28 °C solutions (Figure 1a) and treatment time (Figure 1b). Figure 1a shows that stress tends to increase monotonically with increasing deposition rate (current density); this behavior is generally considered typical for Ni sulfamate plating solutions.[10,19-20] It is also clear from Figure 1a, that activated C treatment lowers stress for all current densities, and that in the current investigation, treatments longer than 4 hours yield only a marginal decrease in film stress over the entire range of current densities. Figure 1 b more clearly illustrates the effect of activated C treatment at the two different current densities examined in the present work, Such carbon treatment removes organic contaminants that may be present in the as-received electrolyte.[20] In order to obtain reproducible stress results when varying other deposition parameters, all electrolytes hereafter studied received a 4 hr C treatment.

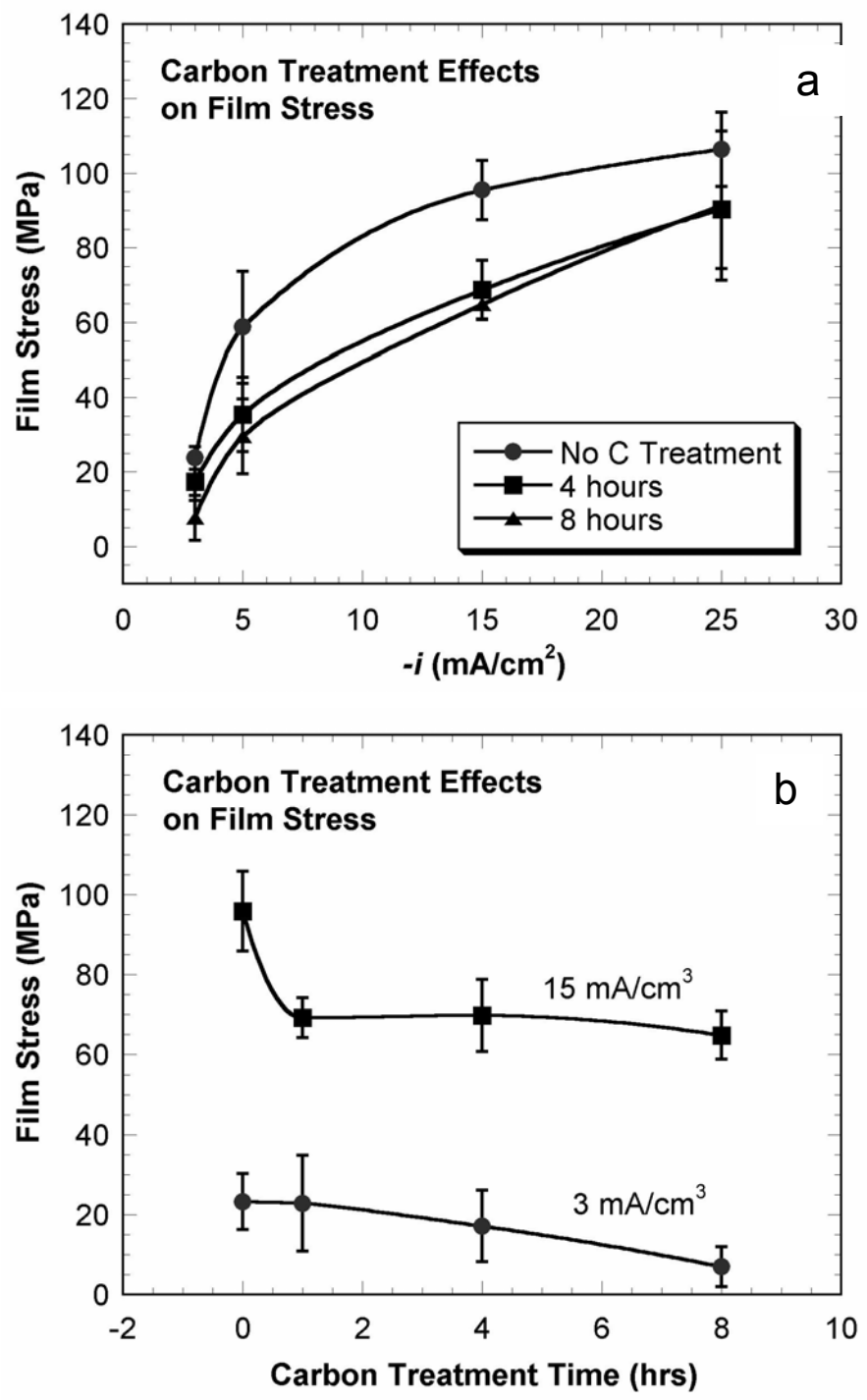

Figure 1. a) Effect of carbon purification treatment on deposited film stress for Ni deposited from a Ni sulfamate electrolyte at 28 °C. Removal of electrolyte impurities shifts film stress towards less tensile values. b) Film stress for 3 and 15 mA/cm^2 as a function of carbon treatment time. The largest effect is observed after just two hours of treatment. Error bars represent the standard deviation of five measurements.

The polarization behavior of treated and untreated electrolytes was investigated to obtain possible insight on mechanism of the treatment's effect on stress. Figure 2 shows the effect of C treatment on deposition polarization behavior using a Pt rotating disk electrode. For current densities less than about 15 mA/cm^2, deposition is somewhat inhibited for the C-treated electrolytes. Other rotation rates were considered, but the degree of inhibition did not seem to be a strong function of rotation rate. This behavior is somewhat counterintuitive, as organics (that are presumably removed *via* purification) are usually thought as inhibiting species for metal deposition. A possible explanation is that the removed contaminants are reduced at the cathode and their removal results in a lower measured current. Another possibility is a more efficient adsorption of other electrolyte species at the cathode (such as sulfamate or borate ions)[21-22] that may act as weak deposition inhibitors.

Electrolyte Filtering Effects

The effect of adding a 5 μm particle filter to the bath circulation pump is shown in Figure 3. Stress at low current densities is dramatically increased with filtering at 28 °C (about a factor of 6 increase for 3 mA/cm^2). The increase in film stress becomes less pronounced with increasing temperature, as shown for 32 and 50 °C in Figures 4 and 5, respectively. Although the data in Figure 3 show that filtering is an important variable at 28 °C, this bath temperature is below the minimum recommended temperature of 32 °C. But Figures 4 and 5 show that at temperatures within the recommended operating range, stress may be affected by simple particle filtering when using low current densities. These results suggest that if low bath temperatures are desired along with low deposition rates, on-off pulse plating with high peak current densities (>15 mA/cm^2) and low duty cycles may be a good approach for avoiding electrolyte handling sensitivities.

The effect of temperature and particle filtering is summarized in Figure 6a which shows the difference in stress, $\Delta\sigma$, between filtered and unfiltered baths for 28, 32, and 50 °C as a function of deposition current density. Values for $\Delta\sigma$ are calculated by subtracting the film stress for unfiltered baths from film stresses in filtered baths (using Figures 3-5). Not surprisingly, for low current densities (<10 mA/cm^2) $\Delta\sigma$ diminishes with increasing bath temperature. In Figure 6b, we show another interpretation of the data in Figures 3 and 4 by plotting the difference in stress values between electrolytes at 28 and 32 °C for unfiltered and filtered baths as a function of current density. We consider these two temperatures since

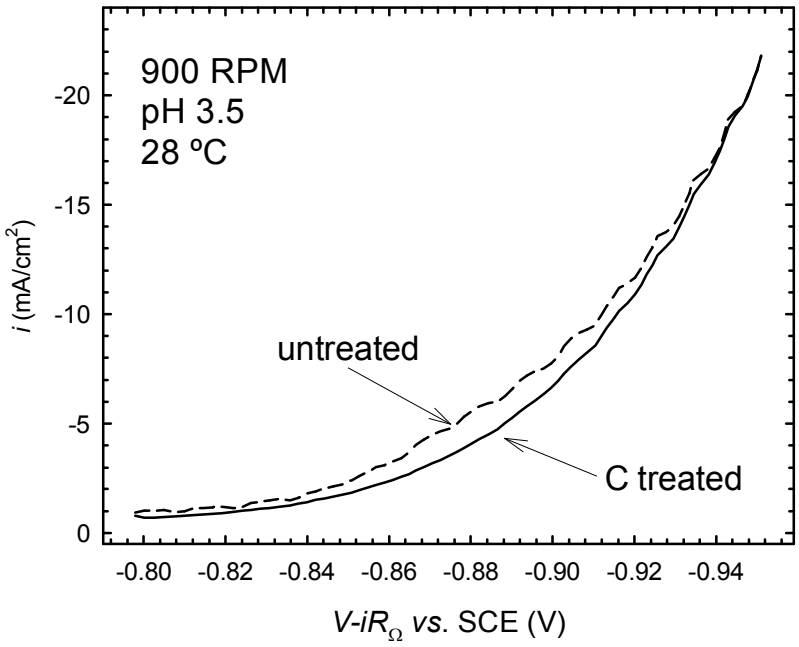

Figure 2. Effect of a two-hour carbon treatment on nickel electrodeposition kinetics on a Pt rotating disk electrode. Potentials are measured relative to saturated calomel electrode (SCE) and corrected for ohmic drop. Carbon treatment results in slightly lower currents at low overpotentials.

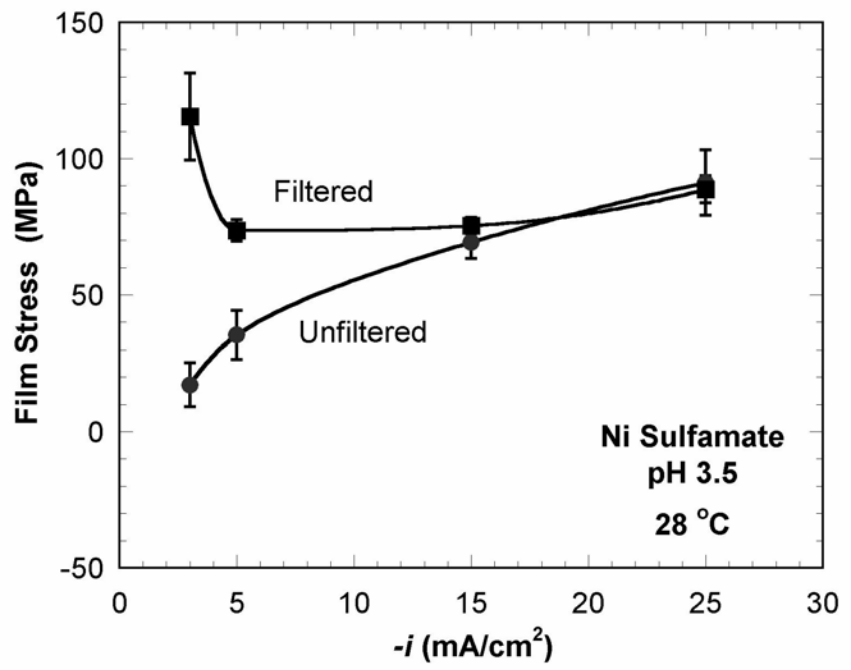

Figure 3. Deposited Ni film stress for filtered and unfiltered electrolytes at 28 °C. Particulate filtering of the electrolyte causes elevated tensile stresses at low current densities. Error bars represent the standard deviation of five measurements

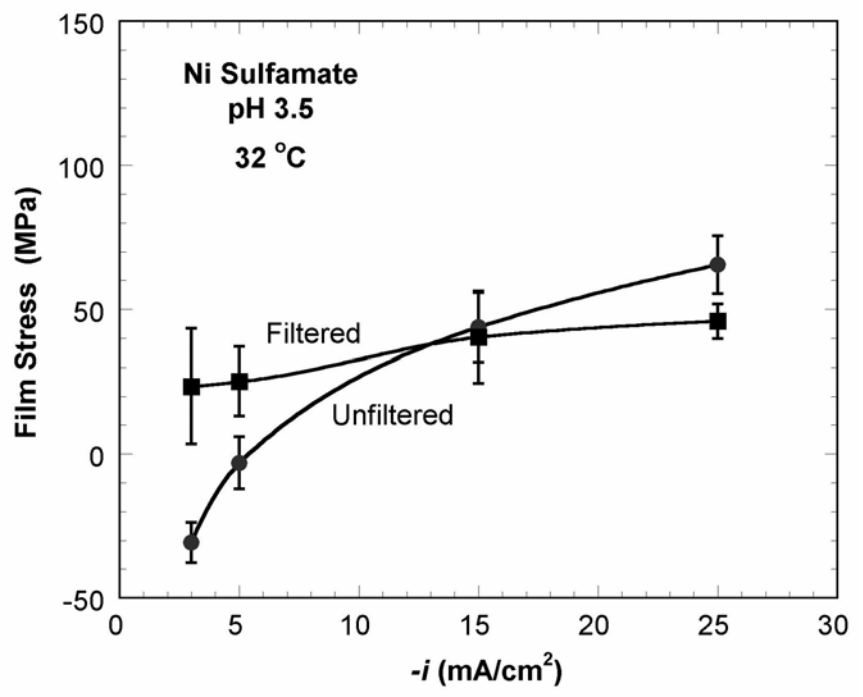

Figure 4. Deposited Ni film stress for filtered and unfiltered electrolytes at 32 °C. The increase in stress observed at low current densities caused by electrolyte filtering is less pronounced at 32 °C. Error bars represent the standard deviation of five measurements.

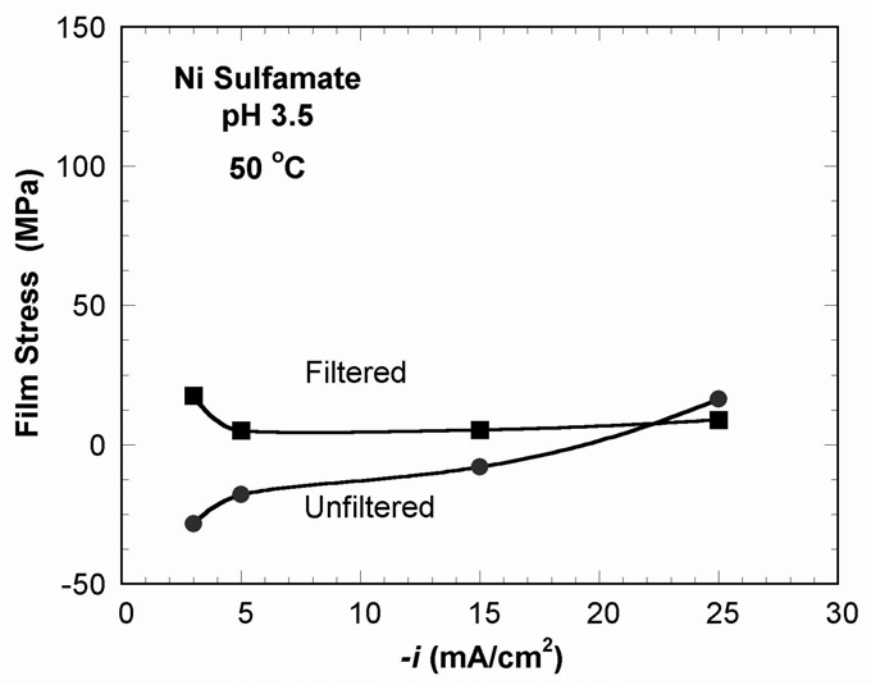

Figure 5. Deposited Ni film stress for filtered and unfiltered electrolytes at 50 °C. Filtering causes just a small increase in film stress at 50 °C. Plotted values are the average of two measurements that were within a few percent of one another.

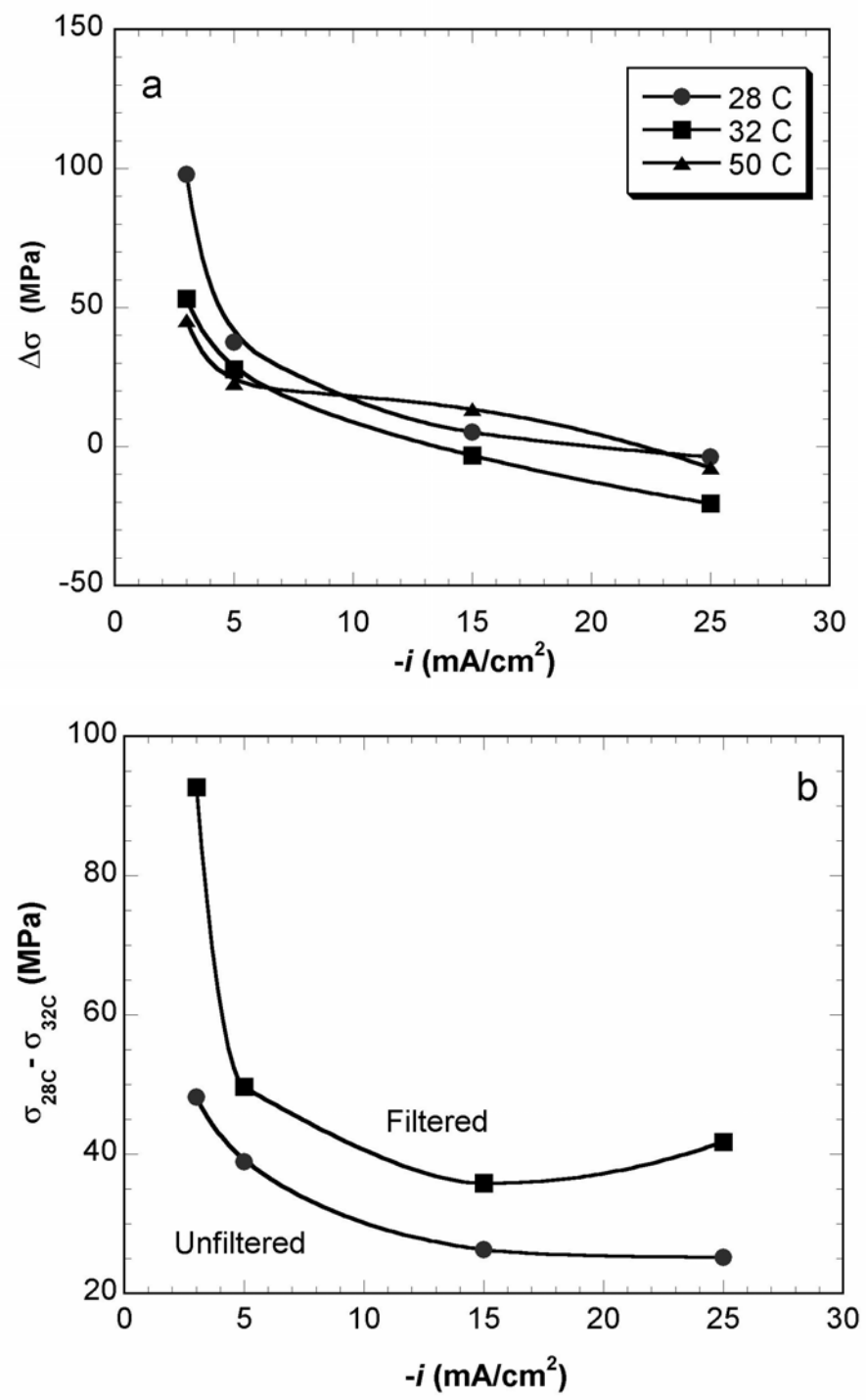

Figure 6. a (top) Film stress difference between deposits from unfiltered and filtered baths $\Delta\sigma$ for different bath temperatures and current densities. Higher bath temperatures lead to lower $\Delta\sigma$ values. b (bottom) Difference in film stress values for deposits obtained in 32 and 28 °C baths, both filtered and unfiltered. Filtering enhances the difference in deposited film stress at 3 mA/cm^2 between the two bath temperatures.

filtering has the largest effect on film stress in this temperature range. Differences in film stress between the two temperatures for unfiltered baths are relatively modest. For filtered baths, Figure 6b shows the remarkably large effect of the deposition temperature on stress as the result of simple particle filtration, especially at low current densities.

Even though such difficulties can be avoided by employing higher current densities, determining the source of the electrolyte handling sensitivity remains of interest. The most obvious possibility is that the filtering removes boric acid from the electrolyte at low temperatures. However, measurements of boric acid content in filtered electrolytes indicated this is not the case. It was also verified that removing the SDS did not affect the behavior shown in Figure 3. After discounting these possibilities, a series of experiments was carried out with different electrolytes to determine the source of the electrolyte handling sensitivity. We first considered the boric acid content of the bath. Results of stress behavior from a Ni sulfamate bath with only 5 g/L of boric acid are shown in Figure 7. Filtering at 28 °C causes only a modest increase of stress at low current densities, as opposed to baths with 30 g/L boric acid. The fact that the filter may be used with only a minor increase in stress indicates that the elevated stress behavior seen with filtering is not due to a contaminant from

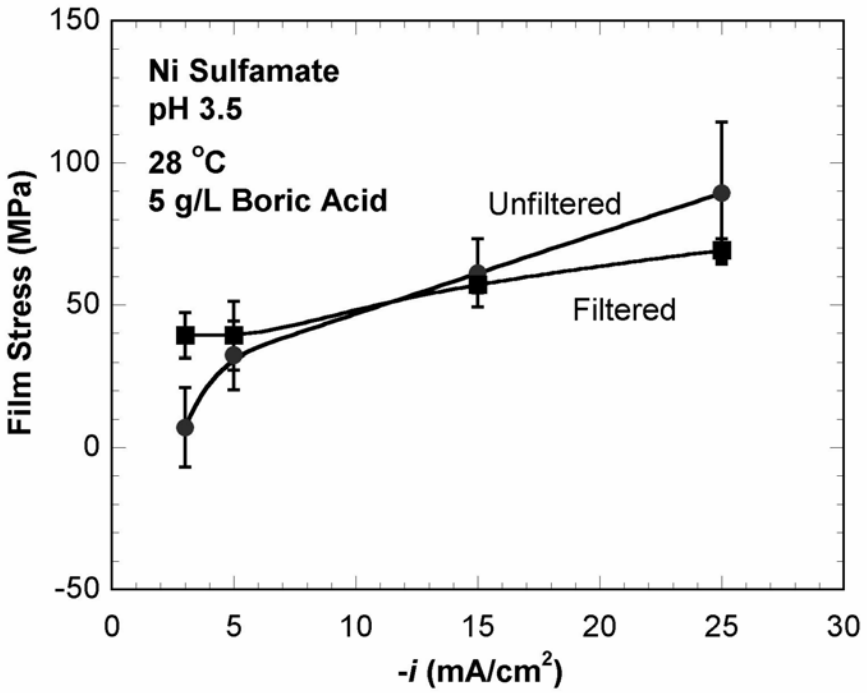

Figure 7. Deposited Ni film stress for filtered and unfiltered electrolytes with only 5 g/L boric acid at 28 °C. Deposition conditions are the same as those used in Figure 3, except the lower boric acid content. With a lower boric acid content, filtering has only a modest effect on film stress values.

the filter itself. Instead, the slight increase observed upon lowering the boric acid content of the bath suggests that the filter-dependent stresses are strongly influenced by the boric acid bath content.

The effect of boric acid concentration is shown another way by plotting the difference in film stress between 30 g/L and 5 g/L boric acid contents for unfiltered and filtered electrolytes in Figure 8. The effect of boric acid content seems to be particularly sensitive to filtering, as the difference in film stress for unfiltered baths is, as would be expected, not strongly dependent on current density. For filtered baths, however, a large increase in stress is apparent for the 30 g/L bath at 3 mA/cm^2. Figure 8 makes clear the important role of the boric acid content of the bath at low temperatures, discussed in more detail below.

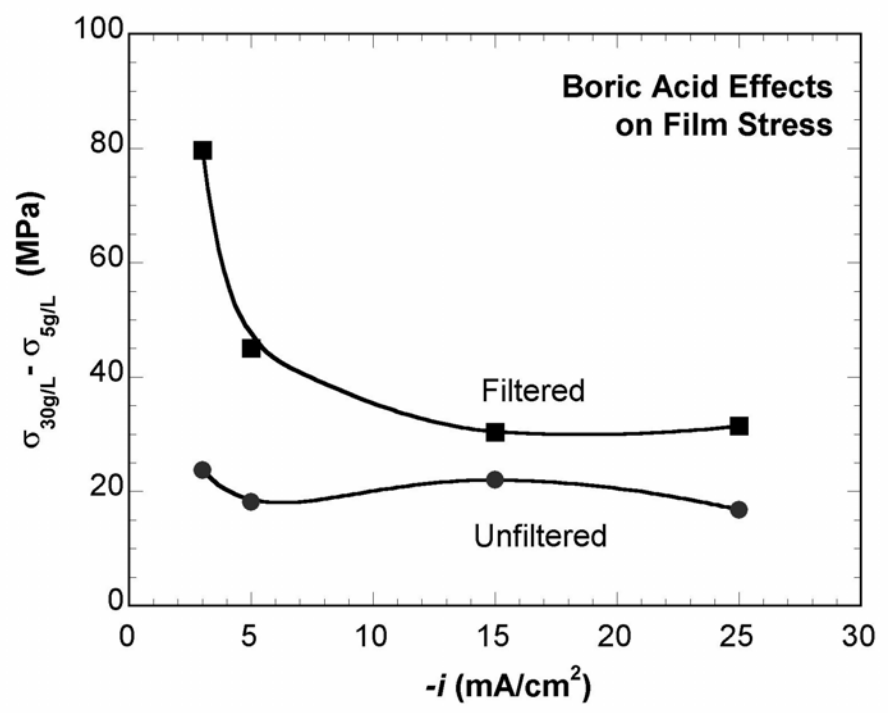

Figure 8. Difference in Ni film stress values for electrolytes having 30 and 5 g/L boric acid for filtered and unfiltered baths. The difference is not a strong function of current density, except for filtered baths, where a large difference observed at 3 mA/cm^2 subsides at higher current densities.

We also considered the importance of the anion of the Ni salt in the film stress behavior by studying a Ni sulfate electrolyte. Figure 9 shows film stresses for a 1.35 M $NiSO_4$ electrolyte with 0.2 g/L SDS and 30 g/L boric acid at a pH of 3.5; a similar increase in film stress is observed upon filtering at 28 °C (about a factor of 4 at 3 mA/cm^2), indicating

that the identity of the anion paired with the Ni^{2+} does not play a large role in elevated stresses seen upon filtering. In fact, for the sulfate electrolyte, the increase in film stress upon filtering is larger than that for the sulfamate electrolyte. These results indicate that the electrolyte handling sensitivity is not a characteristic particular to the sulfamate ion and is instead a more general effect related to the use of boric acid.

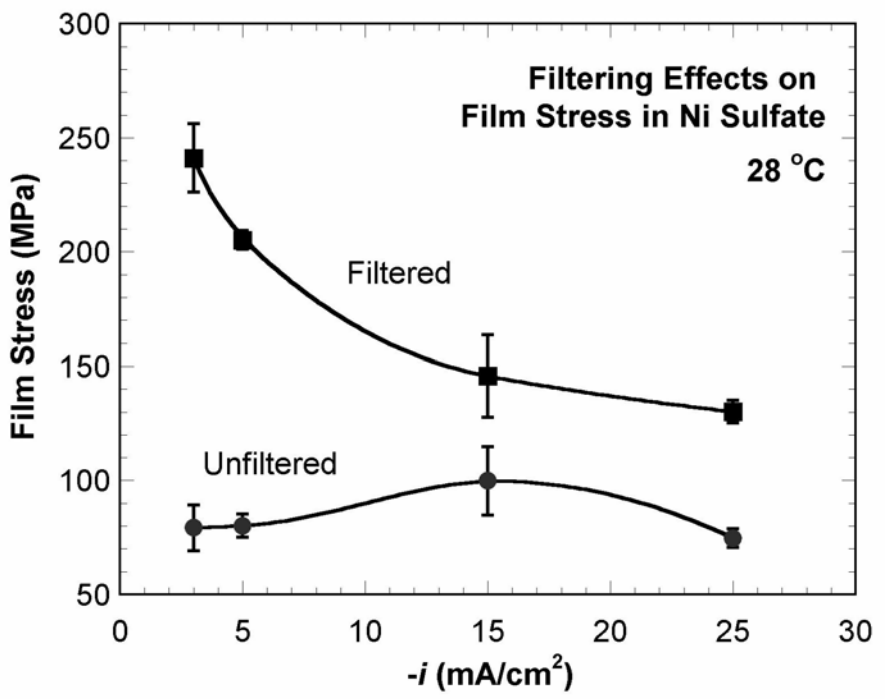

Figure 9. Deposited Ni film stress for filtered and unfiltered 1.35 M Ni sulfate electrolytes with 30 g/L boric acid. Filtering causes higher tensile stress at low current densities for sulfate electrolytes as well.

Since the bath temperature and boric acid content strongly influence the stress for films deposited in filtered baths, we postulate that polyborate ions may be formed during the passage of the electrolyte through the filter material; these polyborate ions would in turn act as weak inhibitors at low deposition rates. At 30 °C, boric acid has an aqueous solubility of 6.23 wt. % (~62 g/L), but the solubility is dependent not only on the ionic strength of the solution but also the nature of its dissolved ions.[23] Upon cooling to about 28 °C, the electrolyte turns from translucent to opalescent; nickel sulfamate solution concentrate is always translucent, even at room temperature. Boric acid, when concentrated, has a tendency to form linkages with itself, resulting in long chains of polyborate ions.[23-24] This precipitation was seen as a white solid collecting on the filter at 28 °C; no solid was visible at higher temperatures. Polyborate formation should be less favored at higher electrolyte temperatures

and lower boric acid bath contents as the boric acid solubility increases. These trends are consistent with the observed trends in stress behavior. Another scenario is a large change in the surface pH for the filtered baths due to a change in the borate chemistry. We will revisit this possibility later when we discuss the results of surface pH measurements.

Interestingly, the difference in stress is only apparent at low current densities; Hoare showed that for low overpotentials boric acid is essential for Ni deposition in sulfate electrolytes.[25-26] He proposed that Ni cations formed a complex with boric acid adsorbed at the cathode through which low-overpotential deposition occurred. In the case of Cu deposition from acid sulfate electrolytes, sulfate ions have been considered as weak inhibitors at low deposition rates.[27-28] Since at low deposition overpotentials film nucleation and growth is more readily affected by adsorbed species,[27] we believe that polyborate ions may act in a similar fashion under these conditions.

Electrolyte Chemistry

The effect of filtering on polarization is shown in Figure 10. At 28 °C, a broad peak starting at –0.5 V *vs*. SCE is evident before the onset of Ni deposition at ~-0.88 V for both filtered and unfiltered electrolytes. This broad peak has been attributed to hydrogen evolution on the Pt surface.[25-26] The current density for filtered electrolytes at low current densities was always lower than that for unfiltered electrolytes. This behavior was extremely reproducible, and may be related to inhibition of the hydrogen evolution or the Ni deposition reactions. Such inhibition is consistent with a species more strongly adsorbed at the cathode in filtered electrolytes. At higher current densities, the difference in polarization between the two baths disappears. This behavior was not a strong function of electrode rotation rate. A similar effect is noted at 32 °C, but the broad peak due to hydrogen was not visible.

Current efficiencies (CE's) were measured by depositing onto a Pt rotating disk electrode, transferring the electrode to a 0.2 M HCl stripping solution, and galvanostatically stripping the Ni deposit at 10 mA/cm^2. Five runs were made for each experimental condition, with the average and standard deviation reported. The endpoint is evident as the potential jumps after the Ni is completely dissolved and oxygen evolution occurs. Table 1 shows the results of measured CE's. There appears to be no large difference in CE between filtered and unfiltered electrolytes at either temperature for the two deposition current densities considered. The low current density of 3 mA/cm^2 has a CE somewhat below 80%, while at 15 mA/cm^2 the CE approaches ~97%. The CE value at 3 mA/cm^2 suggests hydrogen is

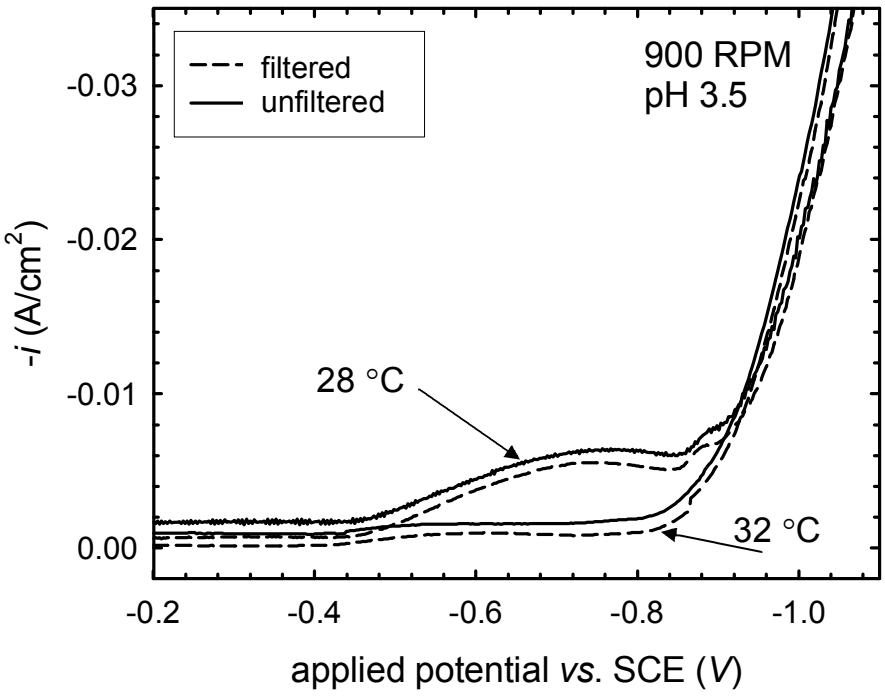

Figure 10. Polarization sweeps for Ni deposition from filtered and unfiltered sulfamate electrolytes at 28 and 32 °C. Deposition current is suppressed at low current densities for filtered baths.

Current Density and Temperature	CE % (Unfiltered)	CE % (Filtered)
3 mA/cm^2 28 °C	77.0 ± 1.1	79.9 ± 1.6
15 mA/cm^2 28 °C	95.6 ± 0.9	94.2 ± 0.5
3 mA/cm^2 32 °C	76.4 ± 0.7	77.8 ± 0.6
15 mA/cm^2 32 °C	96.8 ± 0.8	95.9 ± 0.8

Table 1. Measured current efficiencies (CE) for unfiltered and filtered electrolytes

present at this deposition rate, but the nearly identical 3 mA/cm^2 CE values for both unfiltered (77.0 ± 1.1%) and unfiltered (79.9 ± 1.6%) baths are not consistent with the very different stress behaviors of these baths (see Fig. 3). This is an interesting situation, since stressed Ni deposits at low current densities have been associated with adsorbed hydrogen inhibiting growth;[29] the similar CE's for both low stress and high stress would suggest that the amount of hydrogen generated is the same in both cases.

Although electrolyte handling appeared to have a negligible effect on CE at low deposition rates, it was thought that further insight into the origin of its effect on stress could be gained by studying the pH near the deposition surface. In order to consider this possibility, surface pH measurements were made using a flat-bottomed pH electrode and Au mesh as previously described in the literature.[16-18]

Three different schemes for bringing the Au mesh close to the flat-bottomed pH electrode were considered. In an initial attempt, the Au mesh was mounted on the electrode with adhesive. A second approach entailed mounting the Au mesh in a plastic fixture that could hold the pH electrode. Both approaches were complicated by the fragility of the assembly and the trapping of bubbles on the Au mesh.

The third and ultimately most successful approach entailed employing a loop of 304L stainless steel wire to press the Au mesh against the pH electrode for electrical contact. Only the ring at the bottom touching the mesh was exposed, while the rest of the wire was insulated with shrink wrap and ran up against the side of the electrode where electrical contact was made to the cathode lead. The assembly was mechanically robust and allowed bubbles to escape from the mesh. While all three methods gave similar results, the data shown are from the wire-mesh assembly, which gave the best reproducibility and the least noise. Two runs were made for each condition to ensure reproducibility. We calculated an effective area for the Au mesh as previously described.[16] Before each run, approximately 0.5 μm of Ni was deposited on the Au mesh at 20 mA/cm^2. After waiting a few minutes for the measured pH to stabilize at the bulk pH value, the desired deposition current was set. After each measurement, the plated Ni was cleaned from the Au mesh by gently stripping the plated Ni in a 50% by volume H_2SO_4 solution.

An example of the pH behavior is shown in Figure 11. The curve near the lower part of the figure is the pH electrode response during deposition at 15 mA/cm^2 from a Ni sulfamate electrolyte filtered at 28 °C. The curve near the upper part of the figure is the response from a Ni sulfamate electrolyte with no boric acid. Boric acid has been shown to suppresses hydrogen evolution and stabilize the pH near the cathode during Ni and Ni alloy electrodeposition.[17,32] Thus, when no boric acid is present, the pH rises to about 6. This pH rise for the boric acid-free bath is consistent with previous work with Watts solutions with no boric acid, where pH's between 5 and 7 were attained, depending on Ni^{2+} concentration.[16,33]

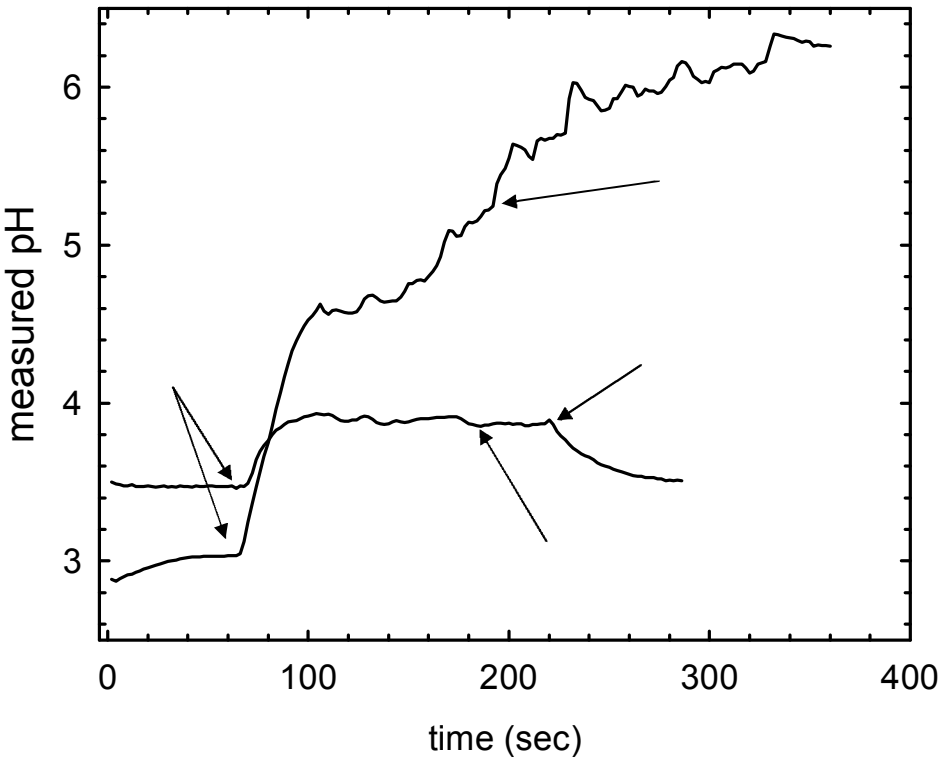

Figure 11. Measurement of pH as a function of time near cathode surface during Ni electrodeposition from sulfamate electrolytes at 28 °C. The curve near the top of the plot illustrates the rapid pH rise during electrodeposition when no boric acid is present, while the second curve at the bottom of the figure shows the relatively small pH rise occurring when boric acid is present (both baths were filtered in this case).

The second curve in Figure 11 shows the pH rise associated with the filtered bath at 28 °C for 15 mA/cm^2. A fairly modest rise from 3.5 to about 3.8 was observed. This behavior is reasonable and in accord with previous measurements using Watts and Ni sulfamate solutions.[4,16] Considering the measurement sensitivity shown in Figure 11, the pH electrode assembly is clearly capable of detecting changes in pH near the surface if they occur.

A summary of all pH measurements is given in Table 2. Response curves for depositions at 3 mA/cm^2 using filtered and unfiltered solutions, are shown in Figure 12. These two conditions are most interesting given the strong differences in film stress previously observed in these cases. Figure 12 shows that pH changes for both conditions are similar and fairly small, from 3.5 to about 3.6. Upon close comparison of Tables 1 and 2, it is

apparent that the filtering-induced changes in CE and pH are consistent; at low current densities, a slight rise in the CE and a smaller increase in pH is noted for filtered baths, while at higher current densities, a lower CE and a larger increase in pH is observed. Electrolyte handling does not have a large effect on surface pH, even under conditions that lead to large changes in film stress. This would suggest that adsorbed hydrogen does not play a role in higher observed film stresses at low deposition rates in filtered baths. We thus attribute such changes in the deposited material not to adsorbed hydrogen but to changes in other adsorbates, most likely polyborates.

Current Density (mA/cm^2)	pH unfiltered	pH filtered
3	3.61 ± 0.01	3.57 ± 0.05
5	3.62 ± 0.02	3.73 ± 0.11
10	3.69 ± 0.02	3.89 ± 0.02
15	3.65 ± 0.02	3.87 ± 0.02

Table 2. Measured pH for different current densities and filtering conditions

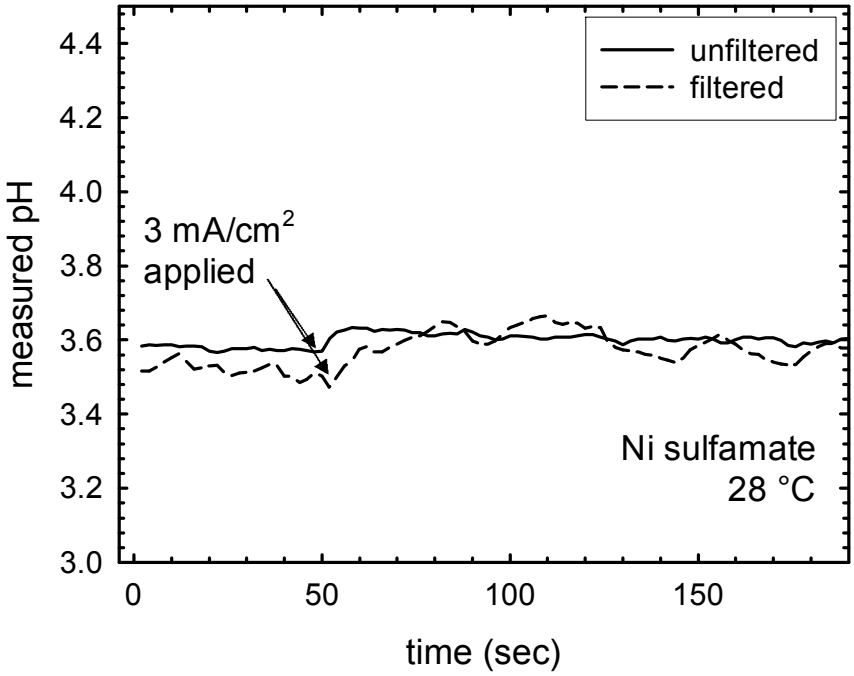

Figure 12. Response of pH near the cathode surface for filtered and unfiltered 28 °C Ni sulfamate baths (both with 30 g/L boric acid) during electrodeposition at 3 mA/cm^2. Despite the large differences in film stress observed for these deposition conditions (see Figure 3), both filtered and unfiltered baths exhibit similar surface pH behavior.

Conclusions

We have shown that at low electrolyte temperatures, boric acid acts as an inhibitor if the electrolyte is handled in such a way as to promote the formation of polyborates. Particle filtering of electrolytes thus becomes an important consideration at low bath temperatures. Higher film stresses are observed at low current densities (<5 mA/cm^2) in low temperature, filtered baths. Despite the large changes in film stress for these conditions, no concomitant differences in pH near the surface are observed. We thus postulate that at low temperatures, electrolyte handling sensitivity is due to the formation of polyborates.

Acknowledgement

The authors thank Dorrance McLean for her support with respect to electrodeposition.

Figure Captions

Figure 1. a (top) Effect of carbon purification treatment on deposited film stress for Ni deposited from a Ni sulfamate electrolyte at 28 °C. Removal of electrolyte impurities shifts film stress towards less tensile values. b (bottom) Film stress for 3 and 15 mA/cm^2 as a function of carbon treatment time. The largest effect is observed after just two hours of treatment. Error bars represent the standard deviation of five measurements.

Figure 2. Effect of a two-hour carbon treatment on nickel electrodeposition kinetics on a Pt rotating disk electrode. Potentials are measured relative to saturated calomel electrode (SCE) and corrected for ohmic drop. Carbon treatment results in slightly lower currents at low overpotentials.

Figure 3. Deposited Ni film stress for filtered and unfiltered electrolytes at 28 °C. Particulate filtering of the electrolyte causes elevated tensile stresses at low current densities. Error bars represent the standard deviation of five measurements.

Figure 4. Deposited Ni film stress for filtered and unfiltered electrolytes at 32 °C. The increase in stress observed at low current densities caused by electrolyte filtering is less pronounced at 32 °C. Error bars represent the standard deviation of five measurements.

Figure 5. Deposited Ni film stress for filtered and unfiltered electrolytes at 50 °C. Filtering causes just a small increase in film stress at 50 °C. Plotted values are the average of two measurements that were within a few percent of one another.

Figure 6. a (top) Film stress difference between deposits from unfiltered and filtered baths $\Delta\sigma$ for different bath temperatures and current densities. Higher bath temperatures lead to lower $\Delta\sigma$ values. b (bottom) Difference in film stress values for deposits obtained in 32 and 28 °C baths, both filtered and unfiltered. Filtering enhances the difference in deposited film stress at 3 mA/cm^2 between the two bath temperatures.

Figure 7. Deposited Ni film stress for filtered and unfiltered electrolytes with only 5 g/L boric acid at 28 °C. Deposition conditions are the same as those used in Figure 3, except the lower boric acid content. With a lower boric acid content, filtering has only a modest effect on film stress values.

Figure 8. Difference in Ni film stress values for electrolytes having 30 and 5 g/L boric acid for filtered and unfiltered baths. The difference is not a strong function of current density, except for filtered baths, where a large difference observed at 3 mA/cm^2 subsides at higher current densities.

Figure 9. Deposited Ni film stress for filtered and unfiltered 1.35 M Ni sulfate electrolytes with 30 g/L boric acid. Filtering causes higher tensile stress at low current densities for sulfate electrolytes as well.

Figure 10. Polarization sweeps for Ni deposition from filtered and unfiltered sulfamate electrolytes at 28 and 32 °C. Deposition current is suppressed at low current densities for filtered baths.

Figure 11. Measurement of pH as a function of time near cathode surface during Ni electrodeposition from sulfamate electrolytes at 28 °C. The curve near the top of the plot illustrates the rapid pH rise during electrodeposition when no boric acid is present, while the second curve at the bottom of the figure shows the relatively small pH rise occurring when boric acid is present (both baths were filtered in this case).

Figure 12. Response of pH near the cathode surface for filtered and unfiltered 28 °C Ni sulfamate baths (both with 30 g/L boric acid) during electrodeposition at 3 mA/cm^2. Despite the large differences in film stress observed for these deposition conditions (see Figure 3), both filtered and unfiltered baths exhibit similar surface pH behavior.

References

1. D. Baudrand, *Metal Finishing*, **94** (7), 15 (1996).

2. J. L. Marti, *Plating*, **53** (1), 61 (1966).

3. Y. Tsuru, M. Nomura, and F. R. Foulkes, *Journal of Applied Electrochemistry*, **30**, 231 (2000).

4. Y. Tsuru, M. Nomura, and F. R. Foulkes, *Journal of Applied Electrochemistry*, **32**, 629 (2002).

5. J. W. Dini and H. R. Johnson, *Thin Solid Films*, **54**, 183 (1978).

6. J. L. Marti and G. P. Lanza, *Plating*, **56** (4) 377 (1969).

7. J. W. Dini and H. R. Johnson, *Surface Technology*, **4**, 217 (1976).

8. B. E. Jacobson and J. W. Sliwa, *Plating and Surface Finishing*, **66** (9), 42 (1979).

9. T. E. Buchheit, D. A. LaVan, J. R. Michael, T. R. Christenson, and S. D. Leith, *Metallurgical and Materials Transactions A*, **33A**, 539 (2002).

10. W. H. Safranek, *The Properties of Electrodeposited Metals and Alloys* (2nd Ed.), American Electroplaters and Surface Finishers Society, U. S. A., 1986.

11. J. W. Dini, *Electrodeposition: The Materials Science of Coatings and Substrates*, Noyes Publications, U. S. A., 1993.

12. C.-S. Lin, K.-C. Peng, P.-C. Hsu, L. Chang, and C.-H. Chen, *Materials Transactions JIM*, **41** (7), 777 (2000).

13. J. W. Dini and H. R. Johnson, *Thin Solid Films*, **54**, 183 (1978).

14. A. Ruzzu, B. Matthis, *Microsystem Technologies*, **8**, 116 (2002).

15. J. J. Kelly, N. Yang, T. Headley, and J. Hachman, *J. Electrochem. Soc*., **150**, C445 (2003).

16. J. Ji, W. C. Cooper, D. B. Dreisinger, and E. Peters, *Journal of Applied Electrochemistry*, **25**, 642 (1995).

17. H. Deligianni and L. T. Romankiw, *IBM J. Res. Develop*., **37** (2), 85 (1993).

18. P. Kern, C. Bonhote, and L. T. Romankiw, *Electrochemical Society Series*, **2002** (27), p. 328 (2003).

19. S. A. Watson, *Nickel Sulphamate Solutions*, NiDI Technical Series 10052, Nickel Development Insitute, Toronto (1989).

20. N. V. Mandich and D. W. Baudrand, *Plating and Surface Finishing*, **89** (9), 68 (2002).

21. J. L .Bubendorff, L. Cagnon, V. Costa-Kieling, J. P. Bucher, and P. Allongue, *Surface Science*, **384**, L836 (1997).

22. E. Chassaing, M. Joussellin, and R. Wiart, *J. Electroanal. Chem*., **157**, 75 (1983).

23. R. A. Smith and R. B. McBroom, *Encyclopedia of Chemical Technology (4th Ed.)*, John Wiley and Sons, U. S. A., p. 365 (1992).

24. F. A. Cotton, G. Wilkinson, C. A. Murillo, and M. Bochmann, *Advanced Inorganic Chemistry* (6th Ed.), John Wiley and Sons, U. S. A., p. 131 (1999).

25. J. P. Hoare, *J. Electrochem. Soc*., **133**, 2491 (1986).

26. J. P. Hoare, *J. Electrochem. Soc*., **134**, 3102 (1987).

27. R. Winand, *Electrochimica Acta*, **39**, 1091 (1994).

28. S. Wu, J. Lipkowski, T. Tyliszczak, and A. P. Hitchcock, *Progress in Surface Science*, **50** (1-4), 227 (1995).

29. J. Amblard, I. Epelboin, M. Froment, and G. Maurin, *Journal of Applied Electrochemistry*, **9**, 233 (1979).

31. T. Fritz, H. S. Cho, K. J. Hemker, W. Mokwa, and U. Schnakenberg, *Microsystem Technologies*, **9**, 87 (2002).

32. J. Horkans, *J. Electrochem. Soc*., **126**, 1861 (1979).

33. Y. Tsuru, R. Takamatsu, and K. Hoskawa, *J. Surf. Finish. Japan*, **44** (1), 39 (1993).

Electrodeposition of Nickel From Low Temperature Sulfamate Electrolytes Part II: Properties and Structure of Electrodeposits

S. H. Goods*, J. J. Kelly**, A. A. Talin*, J. R. Michael***, R. Watson*

Sandia National Laboratories
*Livermore, CA 94551
***Albuquerque, NM 87185

**IBM/T.J. Watson Research Center
Yorktown Heights, NY 10598

Abstract

The structure and properties of Ni films deposited at near-ambient temperatures from sulfamate electrolytes is reported. It is shown that particulate filtering of the electrolyte has significant consequences with respect to the microstructure and resulting material mechanical properties. These effects are most pronounced at low current densities, and gradually disappear as the current density is increased. At the low current density examined (3 mA/cm^2), deposits plated from a particle filtered electrolyte were fine-grained and exhibited a <011> texture orientation, characteristic of "inhibited" growth. The strengths of these finer grain deposits were correspondingly higher, ranging from 700 MPa to nearly 1 GPa; increasing as the deposition temperature increased from 28 ºC to 50 ºC.

Low current density deposits, plated from an unfiltered bath, exhibited a temperature dependent instability in grain morphology and texture. At low temperatures (≤32 ºC) the deposits were coarse grained and predominantly <001>, while at 50 ºC, the deposits were fine grained and <011>. At an intermediate temperature (40 ºC), the deposits grew initially in the uninhibited, coarse grain <001>, but then abruptly transitioned to the fine grain, <011> inhibited growth mode.

In contrast, at the higher current density (15 mA/cm^2), the structure and properties of electrodeposits were unaffected by the presence or absence of particle filtering. Irrespective of deposition temperature or filtering condition, the deposits had the grain morphology and

crystallography characteristics of “uninhibited” growth – namely, coarse, columnar grains with a preferred <001> texture. The measured yield strengths of these deposits were in the 350 MPa to 400 MPa range.

Introduction

Electrodeposition of nickel from sulfamate electrolytes has found wide use in many commercial and industrial applications[1-8] and the rational for its use was described in Part I of this work. More recently, electrodeposited nickel from sulfamate (hereafter referred to as ED Ni-sulfamate) has become a favored material for the electrodeposition of microsystem components using the LIGA process (an acronym for the German words for: lithography, electroplating, and molding). While the LIGA process was introduced in Part I, since the test specimens studied in this second part were fabricated using the LIGA process, we describe it here in some greater detail.

Briefly, a thick (100's to 1000's of microns) polymer photoresist blank, bonded to a metallized substrate (viz., the plating base), is lithographically patterned using a synchrotron X-ray source and developed to yield a mold consisting of deep prismatic cavities having feature sizes measuring in the 10's to 100's of microns. It is into these cavities that an elemental metal or alloy is electrodeposited. As these micro-components may perform mechanical functions, their microstructure and mechanical properties are of interest, as well as the deposition conditions that may affect them. And as stated in Part I, while the process-structure-property relationships are generally known for ED Ni-sulfamate under typical operating conditions[9-10], the successful integration of the electrodeposition step with other steps in the LIGA process may necessitate deposition conditions that differ from standard plating practice.

In particular, it may be necessary to operate plating cells at temperatures, well below those recommended by common practice in order to reduce thermal distortions of the resist material that define the lateral dimensions of a structure.[11] Another aspect that must be considered for the successful integration of the electrodeposition step into the LIGA process is the deposition current density. Transport limitations, particularly important in narrow, high aspect ratio features where circulation of the bulk electrolyte is impeded, are typically minimized by reducing deposition rates. This is most straightforwardly done by depositing metal at low current densities. In this first part of this work, we reported the electrochemistry and process dependence of the intrinsic film stresses of ED Ni-sulfamate over a range of current densities and bath temperatures. In this second part, the effects of these conditions on the mechanical properties and microstructure and of net shape material plated using the LIGA process are presented.

Experimental

Deposition

The composition of the Ni-sulfamate electrolyte is the same as that presented in Part I: 1.35 M $Ni(SO_3NH_2)_2$, 30 g/L boric acid, and 0.2 g/L sodium dodecyl sulfate (as a wetting agent that reduces pitting and otherwise has no effect on the Ni).[12] The deposition parameters for net shape fabrication of test specimens and structures are within the same range of those used for film stress measurements in Part I. In this work, the influence of deposition temperature was examined at 28 °C, 32 °C (the minimum manufacturer recommended deposition temperature), 40 °C and 50 °C. A pH of 3.5 ± 0.1 was used for all deposition runs; the typically recommended range is from 3.5 to 4.5. Particulars related to the preparation of the Ni anodes and the as-received sulfamate electrolyte are described in Part I as well. We do note here though that wound, 5 μm polypropylene fiber filters (Floking) were used as the particle and debris collecting media.

Mechanical Testing

Net shape tensile specimens were fabricated using the LIGA process as described above. Tensile specimens had a reduced gauge section measuring 0. 76 mm x 0.25 mm (width x thickness) and an overall gauge length of 6.2 mm. After final planarization and release from the substrate, the mechanical test specimens were tested in uniaxial tension in an Instron Model 5848 Microtester. Load was measured using a 1 kN load cell and displacement was measured using a non-contacting laser extensometer (EIR Model LE-01) having approximately 1 μm resolution. Tests were performed at room temperature at a constant extension rate of 5×10^{-4} mm/sec.

Microscopy

A FEI DB235 dual beam focused ion beam (FIB) scanning electron microscopy (SEM) was used to characterize the microstructure of as-deposited and heat treated samples employing the ion beam-induced channeling contrast imaging capabilities of the FIB instrument.[13] The depth of penetration of the ions is related to the crystallographic orientation of individual grains. As such, certain crystallographic orientations result in stronger ion channeling and therefore deeper penetration of the ions into the sample. Deeper ion penetration, in turn, produces fewer collectable secondary electrons, so strongly channeling

orientations appear dark as compared to more weakly channeling orientations. The amount of channeling is quite sensitive to small variations (1-2 degrees) in orientation so that not only can grains of different orientations be imaged, but small misorientations within a grain can be visualized as well.

Electron backscatter diffraction (EBSD), performed on a Zeiss Supra 55VP field emission gun SEM using HKL Technology camera and Channel 5 software, was used to map the through thickness grain orientation (texture) of the as-deposited test specimens.

X-ray Characterization

Specimen texture was determined using a Philips X'Pert MRD X-ray diffractometer with a Cu anode operated at 45 kV and 40 mA. Pole figures corresponding to (111), (200), and (220) reflections were collected for azimuthal rotation of $0 \leq \phi \leq 360^{o}$ and tilt angle of $0 \leq \psi \leq 90^{o}$ in 5^{o} increments. The experimental pole figures were corrected for absorption and defocusing using a Ni powder specimen.[14] Based on the experimental pole figures (data only for $\psi \leq 80^{o}$ was used), orientation distribution functions (ODFs) were computed using the BEARTEX program[15]; the ODFs were in turn, used for calculation of inverse pole figures.

Results and Discussion

Filtering effects on Mechanical Properties-

In Part I of this work, it was shown the most pronounced effect of filtering on blanket film stress occurred at low current densities and low plating temperature. Not surprisingly, the as-plated mechanical properties parallel this effect. Figures 1(a) and 1(b) illustrate the typical tensile behavior for electrodeposited test specimens, all plated at 28 ºC and at the current densities and filtering conditions indicated. Stress-strain curves for the material deposited at 3 mA/cm^2 are shown in Figure 1(a). For each filtering condition, the tensile behavior is quite reproducible. Material deposited from an unfiltered bath exhibit yield and ultimate tensile strengths of 350 MP and 500 MPa respectively, similar to the values reported for nickel deposits from a sulfamate bath in the literature.[16-17] It is clear from Figure 1(a), that particle filtering has a significant effect on both the yield and ultimate tensile strength (UTS), with each increasing to 730 and 950 respectively.

Conversely, particle filtering has little effect on the mechanical properties of the electrodeposits when plated at a current density of 15 mA/cm^2 as illustrated in Figure 1b, where tensile curves are presented for each filtering condition. It is evident that, at this

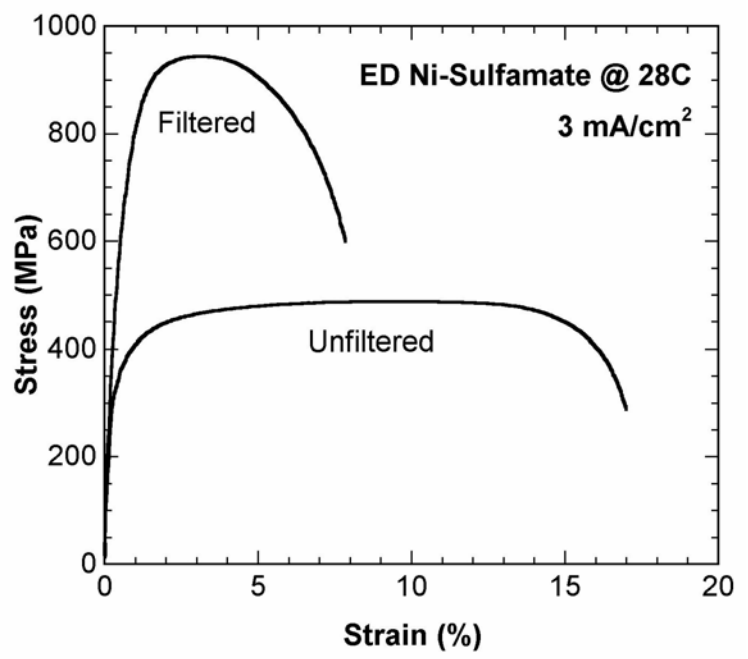

a)

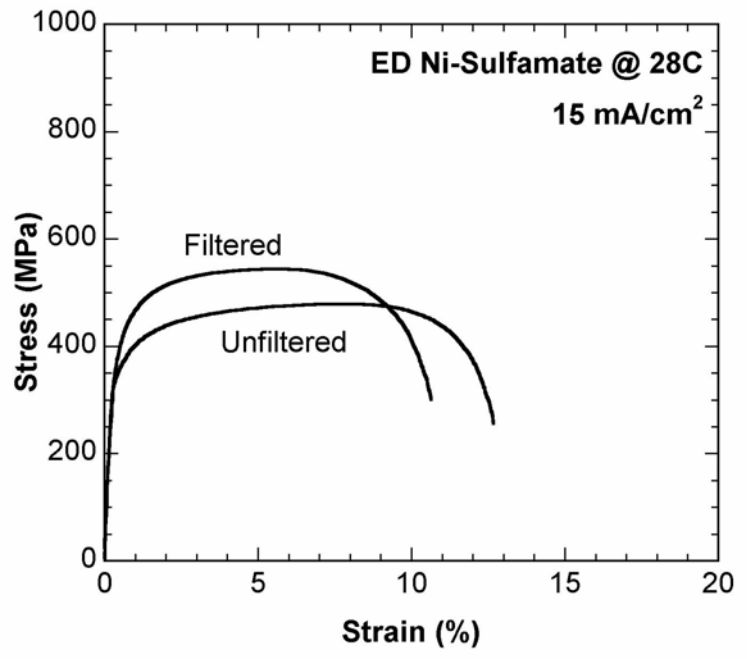

b)

Figure 1. Tensile behavior of electrodeposited nickel from sulfamate electrolytes at 28 ºC. a) High strength is observed in low current density deposits fabricated from particle filtered electrolyte. b) Filtration has little effect on mechanical properties when deposition occurs at higher current density.

higher current density, filtering induces only a small increase in the yield and UTS; 360 MPa and 475 MPa (yield strength) for the material deposited from an unfiltered bath vs. 410 MPa and 540 (UTS) MPa for the material plated from a filtered bath. It is also clear from comparing Figures 1(a) and (b), that current density plays no role in determining mechanical properties in unfiltered baths; both baths yielding material with virtually the same mechanical properties.

Figures 2(a) and (b) illustrate the typical tensile behavior for specimens deposited at the highest temperature 50 ºC. For specimens deposited at the lowest current density, 3mA/cm^2, the presence or absence of filter has no effect on the mechanical properties. Indeed the tensile curve for filtered and unfiltered specimens are essentially indistinguishable from each other. However, these deposits have extremely high strength (note the scale change on the strength axis), as high or higher that that reported in previous literature.[9,16,17] For specimens deposited at 15 mA/cm^2, here too, filtering (or its absence) has no measurable effect on properties. But in this instance strength was low and comparable to that of the specimens deposited at 28C and at the same current density, 15 mA/cm^2.

Figure 3 and Table I summarize the strength measurements for specimens deposited at all temperatures, current densities and bath filtering conditions. It is evident from Figure 3 that the mechanical properties of ED Ni-Sulfamate are insensitive to the presence or absence of particle filtration when plated at the high current density over the entire temperature range examined. For these 15 mA/cm^2 specimens, yield strength is universally low and ranges from about 350 MPa to no higher than 410 MPa. At the low current density however, specimens plating in *unfiltered* cells show a progressive increase in strength as the plating temperature increases. For these specimens, yield strength ranged from 350 MPa at 28 ºC to 950 MPa at 50 ºC. Lastly, the specimens deposited at the low current density from the *filtered* cells show universally high strength with some indication that the strength increases with increasing deposition temperature. In this instance, the yield strength increased from 750 MPa (at 28 ºC) to 900 MPa (at 50 ºC).

Figure 4 compares the intrinsic film stress results from Part I of this work to the current yield strength measurements for ED Ni-sulfamate deposited at 15 mA/cm^2. The previous film stress measurements revealed relatively high stresses (70-75 MPa) for films deposited at the lowest temperature. Figure 4 shows that these film stresses decrease monotonically with increasing deposition temperature for both the filtered and unfiltered electrolyte so that at a deposition temperature of 50 ºC, the film stresses are quite low. In contrast, the yield strengths of the deposits are low for all deposition temperatures and

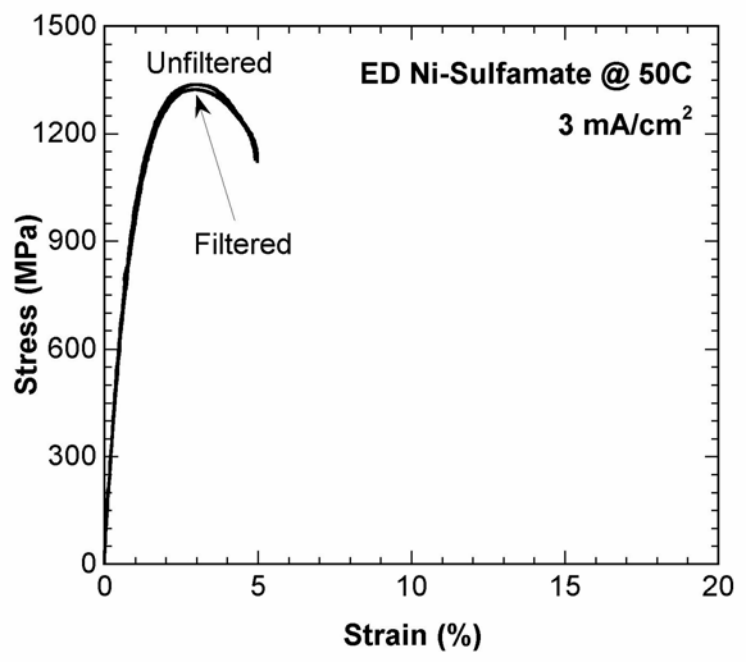

a)

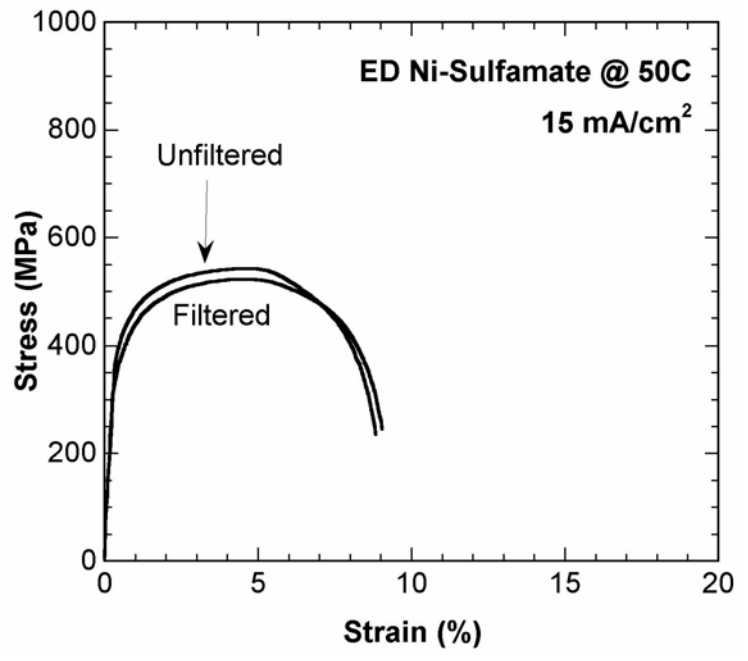

b)

Figure 2. Tensile behavior of electrodeposited nickel from sulfamate electrolytes at 50 ºC. a) High strength is observed in low current density deposits independent of filtering condition. b) Much lower strength is observed in high current density deposits independent of filtering condition.

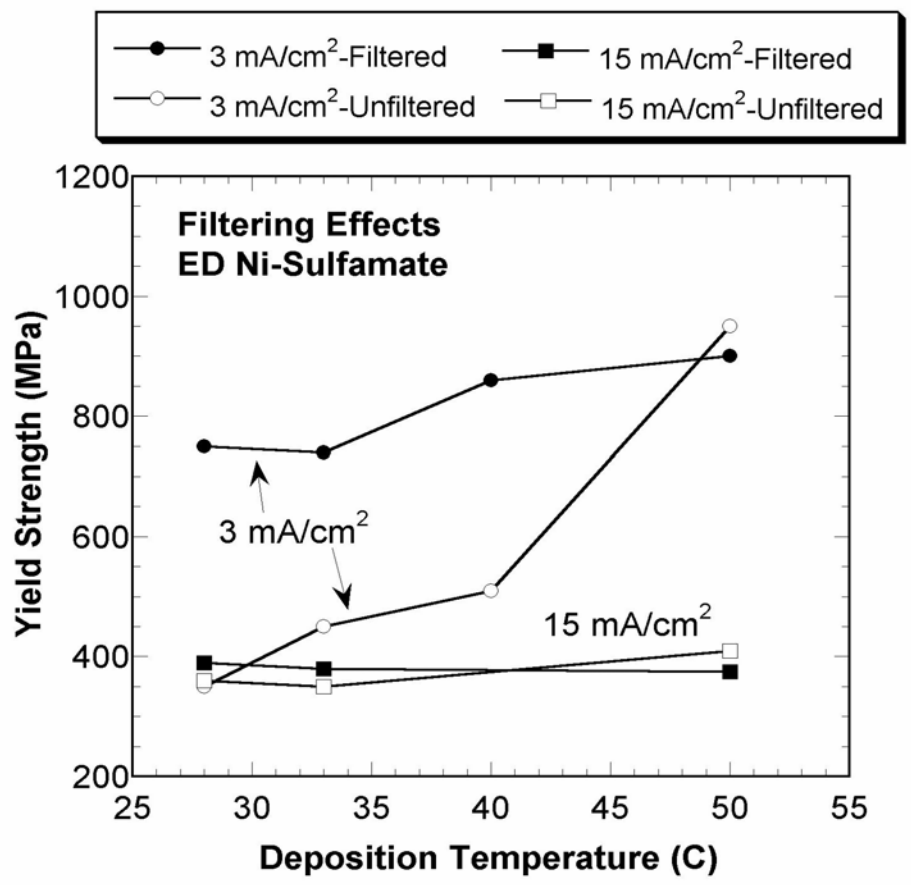

Figure 3. Summary of process parameter effects on strength of electrodeposited nickel from sulfamate electrolytes. High current density deposits always exhibit low strength. Low current density deposits from filtered electrolyte always exhibit high strength. Low current density deposits from unfiltered electrolyte exhibit monotonically increasing strength as deposition temperature increases.

TABLE I. Deposition parameter effects on mechanical properties

Temperature (C)	Current Density (mA/cm^2)	Filtered		Unfiltered	
		YS	UTS	YS	UTS
28	3	750	925	350	490
	15	390	550	360	470
32	3	740	980	450	660
	15	380	500	350	490
40	3	860	1205	505	720
50	3	900	1340	950	1350
	15	375	525	410	540

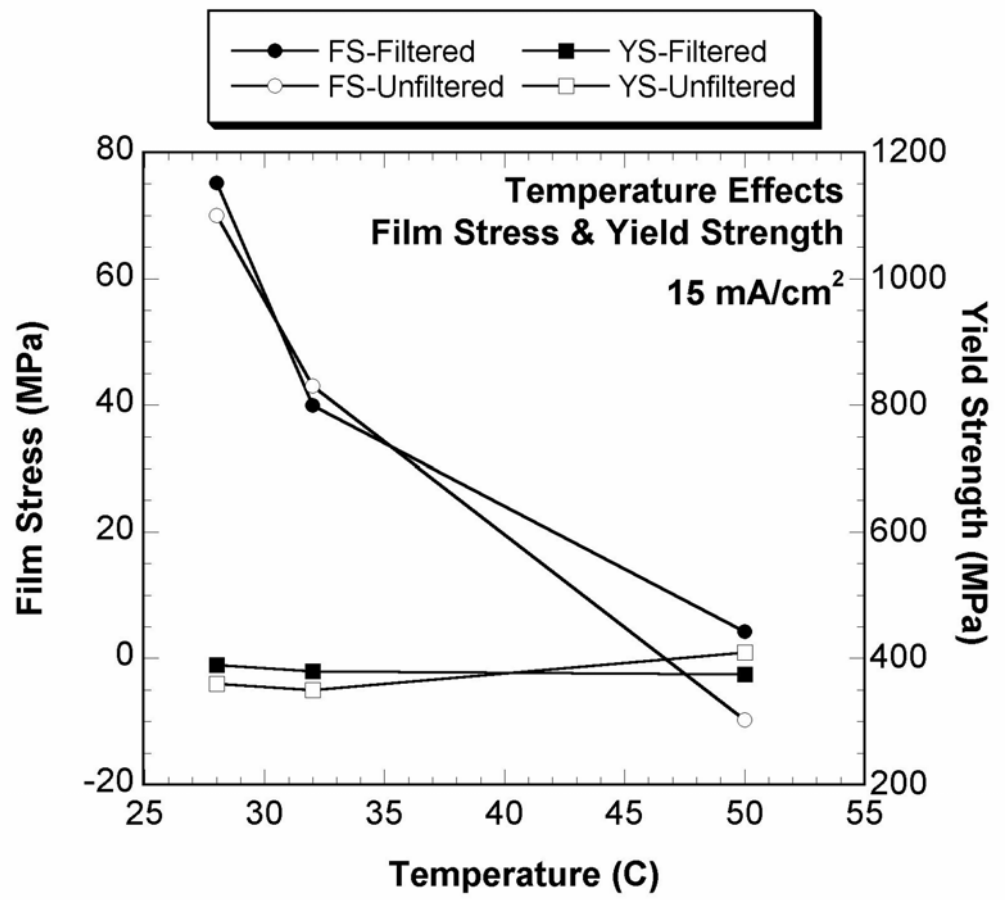

Figure 4. Comparison of intrinsic film strength (FS) and electrodeposit yield strength (YS) for ED Ni-Sulfamate deposited at 50 ºC. Film stress and strength of electrodeposits do not correlate.

filtering conditions. It is evident that there is no correlation between the intrinsic film stress of these deposits and the resultant mechanical properties. Similarly, for other plating conditions (temperature and filtering condition), there is no correlation between the deposit film stress and the strength of the deposited material.

Filtering Effects on Microstructure

Figure 5(a) shows a FIB SEM cross-section for a specimen plated at 3 mA/cm^2 from an unfiltered electrolyte where the plating direction is from the bottom of the image to the top. The coarse, columnar microstructure is typical of ED Ni-Sulfamate plated under conditions where deposition is said to be "uninhibited".[18] We note that the microstructure revealed in this figure is characteristic of the electrodeposits plated from both 15 mA/cm^2 plating cells as well and for the sake of brevity, those micrographs will not be shown. The very bottom of the image includes the initial deposition of nickel upon the metallized LIGA mold substrate. The grain size is initially extremely fine over the first micron or two, but evolves rapidly to the much coarser grain structure that is characteristic of the bulk deposit. This initiation zone where grain size and structure evolve rapidly is commonly observed in electrodeposits. Figure 5(b) shows an EBSD map of this deposit in cross-section (except for the initiation zone). The false color inset is an inverse pole figure (IPF) schematic and indicates that the deposit exhibits a high degree of texture (here texture is referenced to the growth direction normal, that is, the "out-of-plane" texture).* The inset legend reveals that the texture is predominantly <001>, which is also indicative of "uninhibited" growth for ED Ni. Additional texture mapping indicated that all deposits had a field-oriented fiber texture, typical of thick ED's.

Figure 6(a) shows a similar FIB SEM image of the cross-section of a specimen plated at 3 mA/cm^2 in a filtered electrolyte. We note that the initiation zone is still apparent at the bottom of the micrograph but it is evident that the columnar grain size in the bulk is much finer than in the previous instance. This finer grain size is responsible for the considerably higher yield strength.[19] of the deposit as shown in Figures 1 and 3 and is characteristic of inhibited film growth. Inhibited growth in electrodeposits results not only in finer grain size material, but also in a change in the characteristic texture from <001> to <011>. Indeed, the EBSD-derived map shown in Figure 6(b) confirms this change in out-of-plane texture to <011>.

* The EBSD image in Figure 5 and subsequent figures are not purported to be of the precise region shown in the FIB SEM images as both images are obtained from different microscopes requiring intermediate surface preparation. Rather, the EBSD images are taken from the same surfaces as represented by the companion grayscale FIB SEM images.

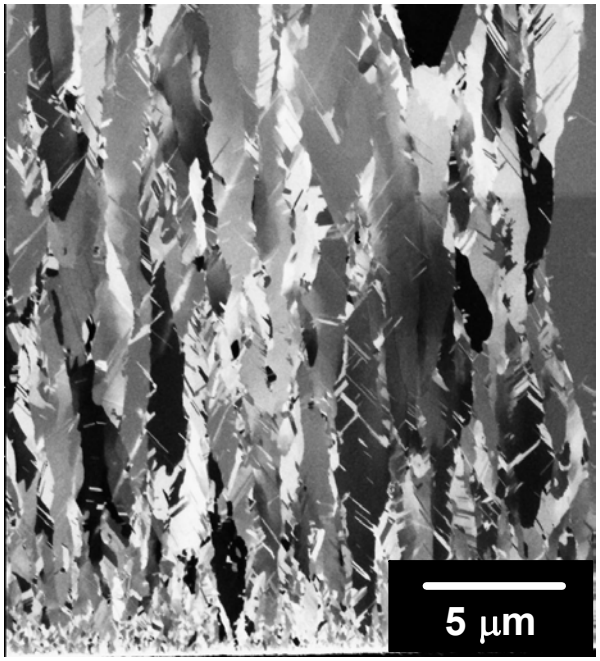

a)

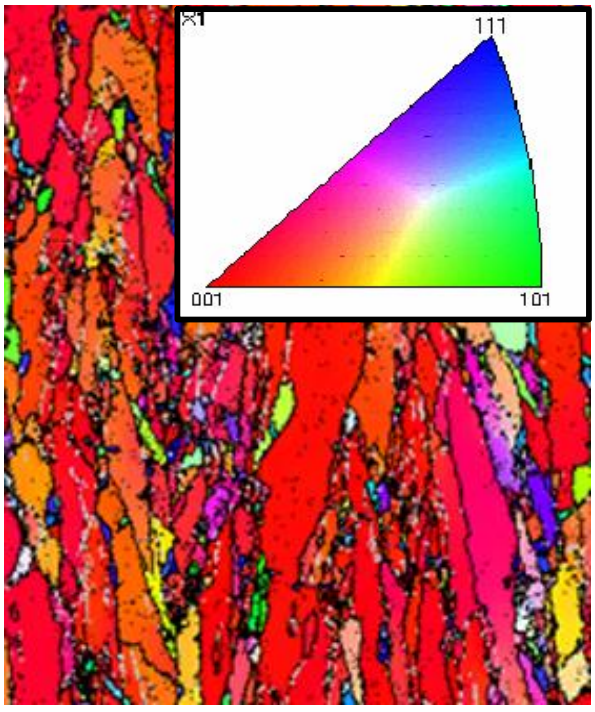

b)

Figure 5. a) FIB-SEM micrograph of electrodeposit cross-section from specimen deposited at 28C, 3mA/cm^2 in unfiltered electrolyte. Deposition direction is vertical in (a) and a finer grain initiation zone is seen at the bottom of the micrograph. b) EBSD map indicates that the microstructure is predominantly <001>. The coarse grain <001> textured microstructure is indicative of uninhibited growth. Specimens from the 15 mA/cm^2 deposits at this temperature exhibited similar grain size and texture.

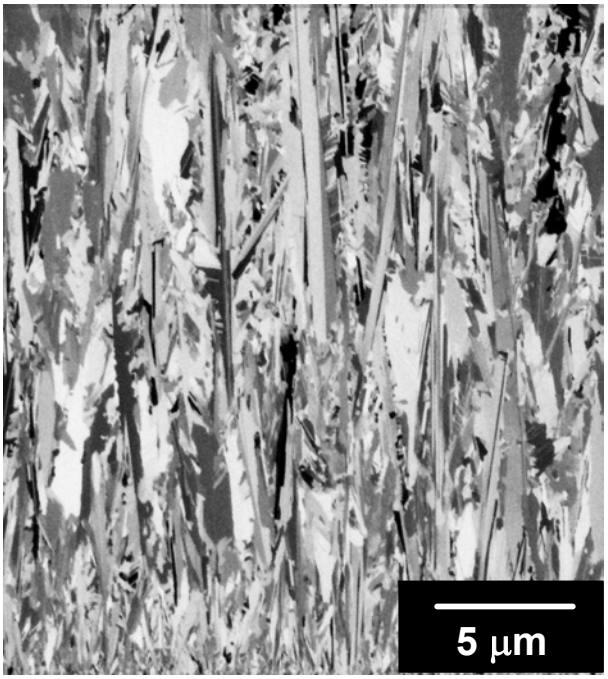

a)

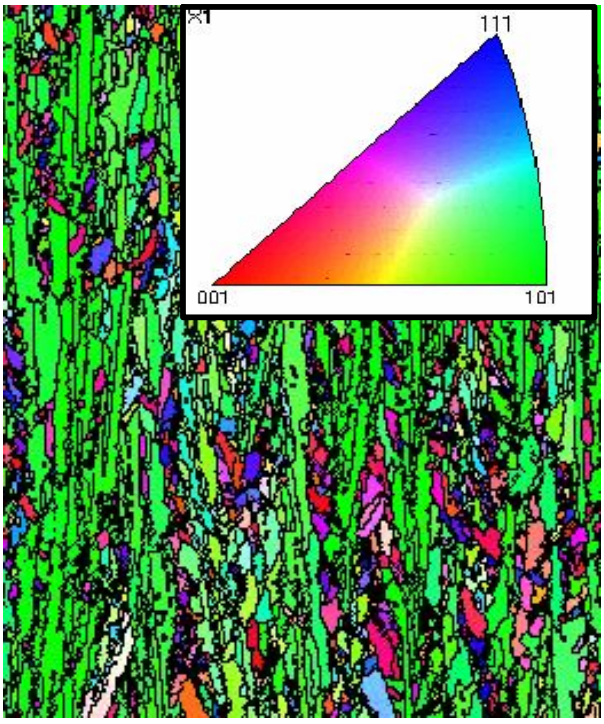

b)

Figure 6. a) FIB-SEM micrograph of electrodeposit cross-section from specimen deposited at 28C, 3mA/cm^2 in filtered electrolyte. Deposition direction is vertical in (a) and the initiation zone of the deposit is seen at the bottom of the micrograph. b) EBSD map indicates that the microstructure is predominantly <011>. The fine grain size and <001> textured microstructure is indicative of inhibited growth.

Figure 7 shows a planview orientation of the same deposit shown in Figure 5(a). Line intercept analysis performed on this SEM image indicated that the average grain size for this electrodeposit was approximately 1.0 μm. The inset in Figure 7 is an x-ray diffraction (XRD) generated IPF that confirms that the preferred texture is <001>. Since XRD samples a larger planar area of deposit that is the case for EBSD, the degree of preferential texture can be assessed more quantitatively. For this deposit, the texture is ≈ 17 times random, indicating a very high degree of texture. Figure 8 shows a similar planview image for a specimen plated under conditions as for the specimen shown in Figure 6a. Line intercept analysis performed on this SEM image indicates that the average grain size for this electrodeposit is nearly five-fold smaller than for the electrodeposit shown in the previous figure, ≈ 200 nm. The IPF inset in Figure 8 confirms the EBSD texture analysis as being <011> and the degree of texturing in this instance was 5 times random. The IPF also gives an indication there is a small amount of texturing associated with higher index direction.

The microstructure of the electrodeposits plated at 50 ºC and 15 mA/cm^2 in both filtered and unfiltered electrolyte exhibit the same characteristics as that shown in Figures 5 and 7, that is coarse grained and <001> textured, characteristic of an uninhibited growth mode for Ni. The only difference observed at 50 ºC (derived from the filtering condition) is a greater degree of preferred orientation for deposit plated from unfiltered electrolyte, 50 times random, vs. 16 times random for the deposit from filtered electrolyte. The coarse grain structure of both of these deposits is reflected in there low yield strength as shown in Figure 3. The 50 ºC deposits plated at 3mA/cm^2 have very high yield strengths and not surprisingly exhibit a fine grain size and <011> texture very similar to that shown in Figures 6 and 8. XRD-derived texture revealed that for the filtered deposit, the <011> texture was 7 times random while for the unfiltered deposit it was 15 time random.

Figure 3 shows that the electrodeposit plated at 40 ºC and at 3mA/cm^2 from an unfiltered electrolyte exhibits a yield strength that is intermediate between that of the high current density deposits and that of the low current density deposit from the filtered electrolyte. It is reasonable therefore to imagine that the microstructure of the deposit would consist of a mixture of the both the coarse-grain, <001> textured material and the fine-grained <011> textured material. Figure 9 shows that this is indeed the case. Here, as in earlier figures, the growth direction is from the bottom to the top of the image. Rather than a

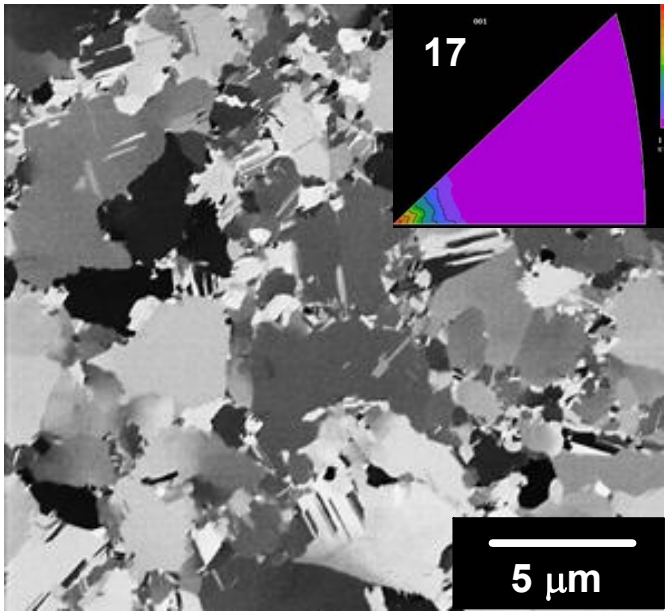

Figure 7. Planview image of deposit shown in Figure 5. XRD-generated IPF inset indicates that the <001> texture is 17 times random.

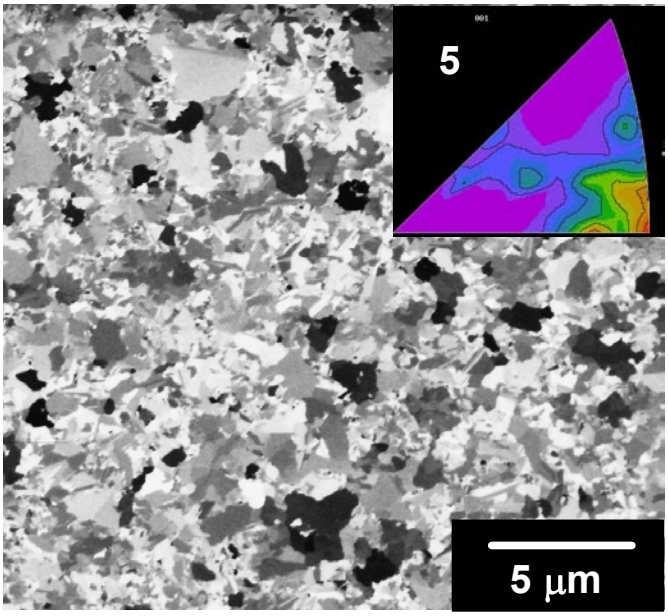

Figure 8. Planview image of deposit shown in Figure 6. XRD-generated IPF inset indicates that the <011> texture is approximately 5 times random

uniform mixture of fine and coarse grained material, leading to the increased strength, Figure 9 shows reveals the deposit to be a duplex in nature consisting of an initially coarse grain columnar structure (disregarding the initiation zone at the very bottom of the micrograph) which abruptly transitions to a fine grained structure at a point very near the mid-thickness of the deposit. Figure 10(a) shows a higher magnification image of the region outlined in Figure 9. The abrupt nature of the transition from coarse grain to fine grain is evident. Figure 10(b) shows an EBSD map of this transition region and reveals that, in concert with the change in grain size, the characteristic texture changes from the <001> free growth texture the <011> texture characteristic of inhibited growth. XRD derived texture of planview sections indicate that the <001> free growth region of the deposit was very highly textured (27 times random) and the <011> inhibited growth region was less strongly, but still significantly textured (6 times random).

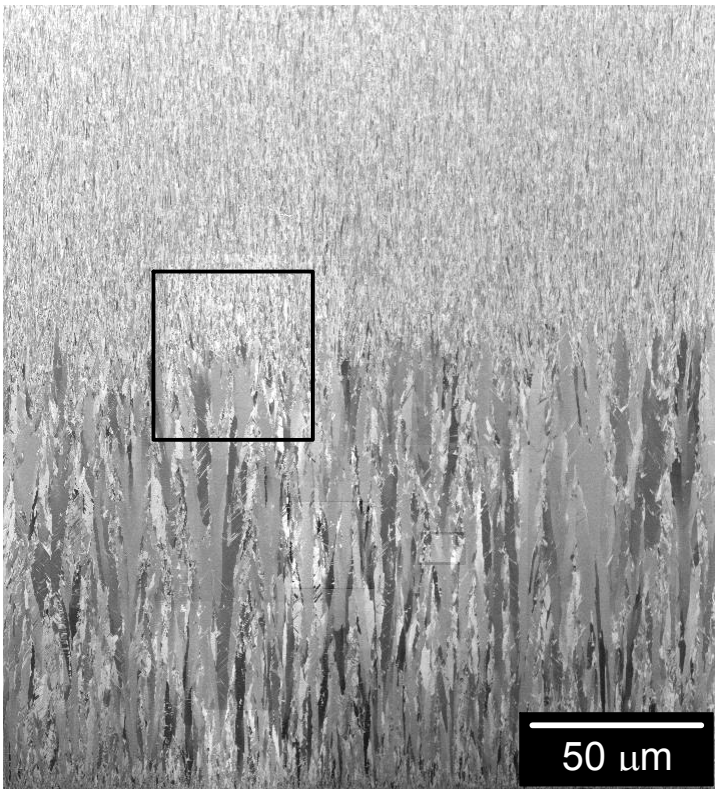

Figure 9. FIB-SEM micrograph of electrodeposit cross-section from specimen deposited at 40 ºC, 3mA/cm^2 in unfiltered electrolyte. The micrograph in the vertical direction spans the entire thickness of the deposit. The deposit is initially coarse grained but abruptly transitions to a fine grain size. The windowed region is shown at higher magnification in Figure 1

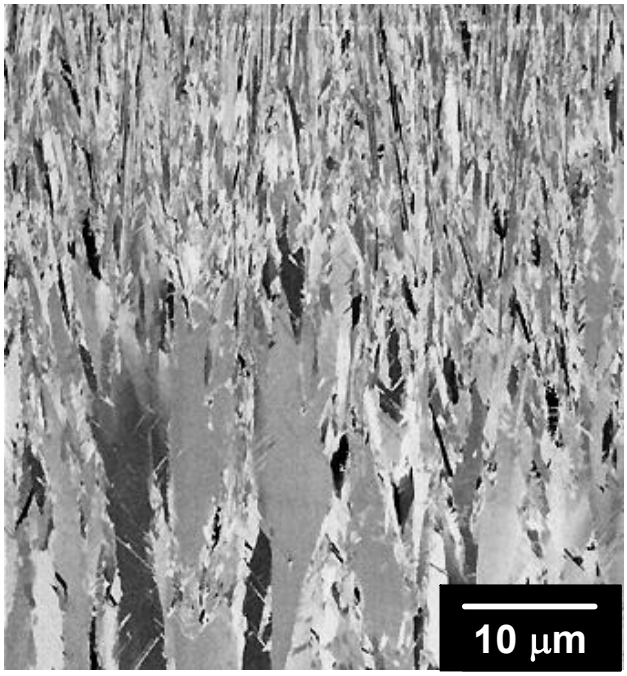

a)

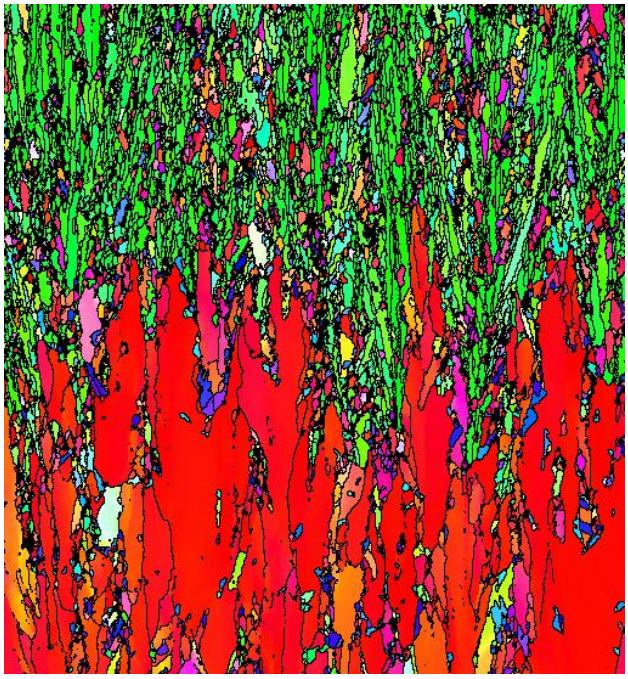

b)

Figure 10. a) Higher magnification FIB-SEM micrograph of region outlined in Figure 9. The abrupt change in grain size is apparent and occurs over about a ten micron region of deposit growth. b) EBSD map indicates that the texture changes from <001> to <011> indicting that the growth mode changes from uninhibited to inhibited during the deposition run.

It seems evident therefore, that the plating parameters established for fabricating this set of specimens result in unstable deposition conditions, allowing the deposit to switch abruptly from coarse grain, highly <001> textured, uninhibited, free growth to a fine grain <011> textured, fully inhibited growth mode. Figure 10 shows that the transition from one growth mode to the other occurs over a very narrow region of about 10 μm and Faradaic considerations indicate that for the 3 mA/cm^2 current density, the switch in growth modes occurs in approximately two hours, out of a total plating time of roughly three days. Sudden changes in film structure, sometimes periodic, that result in non-uniform films or laminate-like films have been previously observed in cross sectional micrographs of electrodeposited Ni.[9] The behavior in Figure 10 demonstrates that, under certain conditions, the microstructure of electroplated Ni may quickly change during the deposition, resulting in a non-uniform through-thickness microstructure. This is presumably due to a change in the nature or type of adsorbed species at the solid-liquid interface such as hydrogen and hydroxides (see below), electrolyte aging species, or species from other chemical reactions occurring in the bulk electrolyte all of which may result in a change in the film nucleation and growth,

It is clear that in all instances, coarse grained deposits are associated with the <001> texture indicative of free growth while fine grained deposits are associated with the characteristic <011> inhibited growth mode. Rationalizing all of the various observations presented above with respect to growth mode, deposition parameters and electrolyte condition is difficult. Inhibition during electrodeposition is usually attributed to the presence of an adsorbate, suppressing growth of a certain orientation and promoting the growth of other orientations.[18, 20, 21] The degree to which such an adsorbate is bound to the growing surface determines, at least to some extent, the temperature and current density regime in which inhibited growth is observed. The insensitivity of the 15 mA/cm^2 deposits with respect to plating conditions can be rationalized in a relative straightforward manner in that at this higher current density, any inhibiting species that may be present (hydrogen or adsorbed boric acid species, as examples) is simply overwhelmed by the high deposition rate. Deposition at this current density therefore always occurs in the free growth mode, regardless of the other plating parameters investigated here; temperature and electrolyte filtration. Similarly, for the electrodeposits plated at 3 mA/cm^2 from filtered electrolyte, deposition is sufficiently slow so as to allow even a weakly bound adsorbate to remain effective in inhibiting growth. Amblard et al. investigated texture evolution in Ni-Watts electrodeposits plated at 50^{o}C, and observed a

similar transition from fine-grain, <011> oriented (at pH<2.5) and <112> oriented (pH>2.5) growth to coarse-grain, <001> oriented growth as current density increased above ~5 mA/cm^2. [20] These authors argued that at lower current density adsorbed hydrogen or $Ni(OH)_2$ inhibited <001> growth, while stabilizing <001> and <112> orientations, leading to deposits with these textures. In the present case it is unclear why particle filtering should affect the growth mode, since no change in pH near the cathode upon filtering the electrolyte was observed in Part I of this work.

It is difficult to postulate a single mechanism that can account for the structure and texture of the deposits plated from the unfiltered electrolyte at 3 mA/cm^2. At the lowest deposition temperature, the coarse grain <001> texture observed in the 3 mA/cm^2 deposit from the *unfiltered* electrolyte implies free growth and the absence of any inhibiting species, much like both of the deposits plated at the same temperature, but at the higher current density. However, compared to the companion deposit from the *filtered* electrolyte at 28 ºC and 3 mA/cm^2, it is apparent that the deposition conditions at the metal/electrolyte interface are directly related to the presence or absence of particle filtration in a way that is not obvious. It appears that particle filtration of the sulfamate/boric acid electrolyte promotes the formation of a species that effectively inhibits deposition. Absent the filtration at this temperature and current density, uninhibited growth is the preferred mode.

Most problematic though, is rationalizing the character of the 50 ºC, 3 mA/cm^2 deposit from the *unfiltered* electrolyte. The fine grain microstructure and <011> preferred orientation of this deposit suggests the presence of an effective adsorbed inhibiting specie at the higher temperature that is not present at the lower temperature. Lin et al, who investigated effects of increased ammonium ion concentration on sulfamate Ni deposits also observed a similar trend in texture and microstructure as bath temperature was increased from 40°C to 50°C.[22] It is not evident why higher deposition temperatures would lead to increased inhibition at low current densities. One is left then, with postulating the presence of a second, additional mechanism, perhaps the increased adsorption of a certain sulfamate electrolyte species only at high temperatures and low deposition rates, resulting in inhibited growth under such conditions.

Such a mechanism would help one understand the instability in growth mechanism observed in the 40 ºC 3 mA/cm^2 deposit from the unfiltered electrolyte. Given that this temperature is midway between the inhibited and uninhibited growth regimes, this instability would not be surprising since small perturbations in the growth conditions would translate to major changes in the structure of deposit.

Conclusions

The structure and properties of nickel deposited from sulfamate electrolytes has been shown to be sensitive to a variety of processing parameters including: current density, deposition temperature and electrolyte conditioning (particle filtration). The effects are particularly apparent at low applied current density. At 3 mA/cm^2, deposition from *filtered* electrolyte yields material that is fine grained and predominantly <011> textured; characteristic of inhibited growth. At 15 mA/cm^2, ED nickel sulfamate deposits are coarse grain and exhibit predominantly <001> texture characteristic of free or unihibited film growth irrespective of filtering condition. Low current density deposits from *unfiltered* electrolyte are coarse grained and <001> textured when plated at 28C, characteristic of free or uninhibited growth but are similar in grain morphology and texture to their filtered counterparts when plated at 50C. At intermediate temperatures, deposits exhibit a dramatic instability in growth mode, growing initially in a free growth mode but then rapidly transitioning to an inhibited growth mode.

The mechanical properties of these deposits track with their grain size; the fine grain deposits resulting from inhibited growth exhibit yield strengths between approx. 750-950 MPa while larger grain size deposits resulting from uninhibited growth exhibit yield strengths between approx. 350 and 400 MPa.

Acknowledgements

The authors thank Dorrance McLean and John Hachman for their assistance in the fabrication of the test specimens used in this study as well as Andy Gardia, Michael Rye, Bonnie McKenzie for their assistance in metallographic preparation and microscopy.

Figure Captions

Figure 1. Tensile behavior of electrodeposited nickel from sulfamate electrolytes at 28 ºC. a) High strength is observed in low current density deposits fabricated from particle filtered electrolyte. b) Filtration has little effect on mechanical properties when deposition occurs at higher current density.

Figure 2. Tensile behavior of electrodeposited nickel from sulfamate electrolytes at 50 ºC. a) High strength is observed in low current density deposits independent of filtering condition. b) Much lower strength is observed in high current density deposits independent of filtering condition.

Figure 3. Summary of process parameter effects on strength of electrodeposited nickel from sulfamate electrolytes. High current density deposits always exhibit low strength. Low current density deposits from filtered electrolyte always exhibit high strength. Low current density deposits from unfiltered electrolyte exhibit monotonically increasing strength as deposition temperature increases.

Figure 4. Comparison of intrinsic film strength (FS) and electrodeposit yield strength (YS) for ED Ni-Sulfamate deposited at 50 ºC. Film stress and strength of electrodeposits do not correlate.

Figure 5. a) FIB-SEM micrograph of electrodeposit cross-section from specimen deposited at 28C, 3mA/cm^2 in unfiltered electrolyte. Deposition direction is vertical in (a) and a finer grain initiation zone is seen at the bottom of the micrograph. b) EBSD map indicates that the microstructure is predominantly <001>. The coarse grain <001> textured microstructure is indicative of uninhibited growth. Specimens from the 15 mA/cm^2 deposits at this temperature exhibited similar grain size and texture.

Figure 6. a) FIB-SEM micrograph of electrodeposit cross-section from specimen deposited at 28C, 3mA/cm^2 in filtered electrolyte. Deposition direction is vertical in (a) and the initiation zone of the deposit is seen at the bottom of the micrograph. b) EBSD map indicates that the

microstructure is predominantly <011>. The fine grain size and <001> textured microstructure is indicative of inhibited growth.

Figure 7. Planview image of deposit shown in Figure 5. XRD-generated IPF inset indicates that the <001> texture is 17 times random.

Figure 8. Planview image of deposit shown in Figure 6. XRD-generated IPF inset indicates that the <011> texture is approximately 5 times random

Figure 9. FIB-SEM micrograph of electrodeposit cross-section from specimen deposited at 40 ºC, 3mA/cm^2 in unfiltered electrolyte. The micrograph in the vertical direction spans the entire thickness of the deposit. The deposit is initially coarse grained but abruptly transitions to a fine grain size. The windowed region is shown at higher magnification in Figure 1

Figure 10. a) Higher magnification FIB-SEM micrograph of region outlined in Figure 9. The abrupt change in grain size is apparent and occurs over about a ten micron region of deposit growth. b) EBSD map indicates that the texture changes from <001> to <011> indicting that the growth mode changes from uninhibited to inhibited during the deposition run.

References

1. D. Baudrand, *Metal Finishing*, **94** (7), 15 (1996).

2. J. L. Marti, *Plating*, **53** (1), 61 (1966).

3. Y. Tsuru, M. Nomura, and F. R. Foulkes, *Journal of Applied Electrochemistry*, **30**, 231 (2000).

4. Y. Tsuru, M. Nomura, and F. R. Foulkes, *Journal of Applied Electrochemistry*, **32**, 629 (2002).

5. T. E. Buchheit, D. A. LaVan, J. R. Michael, T. R. Christenson, and S. D. Leith, *Metallurgical and Materials Transactions A*, **33A**, 539 (2002).

6. J. L. Marti and G. P. Lanza, *Plating*, **56** (4) 377 (1969).

7. J. W. Dini and H. R. Johnson, *Surface Technology*, **4**, 217 (1976).

8. B. E. Jacobson and J. W. Sliwa, *Plating and Surface Finishing*, **66** (9), 42 (1979).

9. W. H. Safranek, *The Properties of Electrodeposited Metals and Alloys* (2nd Ed.), American Electroplaters and Surface Finishers Society, U. S. A., (1986).

10. J. W. Dini, *Electrodeposition: The Materials Science of Coatings and Substrates*, Noyes Publications, U. S. A., (1993).

11. A. Ruzzu, B. Matthis, *Microsystem Technologies*, **8**, 116 (2002).

12. J. W. Dini and H. R. Johnson, *Thin Solid Films*, **54**, 183 (1978).

13. J. I. Goldstein et al, Scanning Electron Microscopy and X-ray Microanalysis, Kluwer Academic/Plenum Publishing, New York, 2003, p.558

14. U. F. Kocks, C. N. Tome, and H. R Wen, . Texture and Anisotropy, Preferred Orientation in Polycrystals and their Effect on Materials Properties, Cambridge U. Press, (1998)

15. http://eps.berkeley.edu/~Wenk/TexturePage/beartex.html

16. K. J Hemker, H. Last, Microsample Testing of LIGA Nickel for MEMS Applications, Materials Science and Engineering, **A319-321**, 882, (2001)

17. H.S. Cho, K.J. Hemker, K. Lian, J. Goettert, G. Dirras, Measured Mechanical Properties of LIGA Nickel Structures, Sensors and Actuators A, **59**, (2003)

18. H. Fischer, Electrodeposition and Surface Treat. 1, 319 (1973)

19. E. O. Hall, *Proc. R. Soc. London*, **64**, 747 (1951)

20. J. Amblard, I. Epelboin, M. Froment, and G. Maurin, J. Appl. Electrochem. 9, 233, (1979)

21. C. B. Nielsen, A. Horsewell, and M. J. L. Ostergard, J. Appl. Electrochem. 27, 839 (1997)

22. C. S. Lin, P. C. Hsu, L. Chang, C. H. Chen, J. Appl. Electrochem. 31, 925 (2001)

Distribution List

5 James Kelly
IBM/T.J. Watson Research Center
P.O. Box 218
Yorktown Heights, N.Y. 10598

1	MS 9004	Hruby, Jill, 08100
1	MS 9405	Carling, Bob 08700
1	MS 9161	Even, Bill, 08760
1	MS 9404	Kubiak, Glenn, 08750
1	MS 9042	Chen, Er-Ping, 08763
1	MS 9042	Kwon, Davina, 08774
1	MS 9042	Forman, Michael, 08774
1	MS 9161	Griffiths, Stewart, 08350
1	MS 9161	Medlin, Doug, 08761
1	MS 9161	Dibble, Dean, 08761
1	MS 9161	Marquis, Emmanuel, 08761
1	MS 9161	McCarty, Kevin, 08761
1	MS 9161	Lee, Jean, 08764
1	MS 9401	Aigeldinger, George, 08753
1	MS 9401	Allendorf, Sarah, 08753
1	MS 9401	Boehme, Dale, 08753
1	MS 9401	Ceremuga, Joe, 08753
1	MS 9401	Hachman, John, 08753
1	MS 9401	Hekmaty, Michelle, 08753
1	MS 9401	Hunter, Luke, 08753
1	MS 9401	Losey, Matthew, 08753
1	MS 9401	Mclean, Dorrance, 08753
1	MS 9401	Malinowski, Mike, 08753
1	MS 9401	Mrowka, Stan, 08753
1	MS 9401	Yang, Peter, 08753
1	MS 9401	Skala, Dawn, 08753
3	MS 9401	Talin, Alec, 08764
1	MS 9402	Goldsmith, John, 08772
1	MS 9403	Mills, Bernice, 08773
1	MS 9403	Yang, Nancy, 08773
1	MS 9403	Wang, Jim, 08773
1	MS 9403	Morales, Alfredo, 08762
10	MS 9409	Goods, Steve, 08754
1	MS 9409	Jin, Helena, 08754
1	MS 9409	Lee, Sangwook, 08754
1	MS 9409	Lu, Wei Yang, 08754
1	MS 9409	McFadden, Sam, 08754
1	MS 9409	Spence, Paul, 08754
1	MS 9409	Watson, Roger, 08754
1	MS 9409	Evans, Greg, 08775
1	MS 9409	Larson, Rich, 08775

1 MS 9953 Haroldsen, Brent, 08755

SNL/NM
1 MS 0889 Boyce, Brad, 01824
1 MS 0889 Buchheit, Tom, 01824
3 MS 0886 Michael, Joe, 01822
1 MS 0889 Prasad, Somuri, 01824
1 MS 1415 Hearn, Sean, 01112
1 MS 1310 Mitchell, John A., 02614
1 MS 0311 Wild, Ron, 02618
1 MS 0311 Vanacek, Carl, 02618
1 MS 0311 Petersen, Daniel, 02618

Honeywell Federal Manufacturing And Technologies
1 MS-MD40 Zawiki, Larry
1 MS-MD40 Widmer, Madhuri
1 MS-FH40 Dearth, Bob
P.O. Box 419159
Kansas City, MO. 64141-6159

3 MS 9018 Central Technical Files, 8945-1
1 MS 0899 Technical Library, 9616
1 MS 9021 Classification Office, 8511 for Technical Library, MS 0899, 9616
DOE/OSTI via URL (List on the Distribution list as shown here, but do not send a hard copy. A copy will be sent electronically by the R&A process.)